High-resolution temporal and stratigraphic record of Siletzia's accretion and triple junction migration from nonmarine sedimentary basins in central and western Washington

Michael P. Eddy[1,†], Samuel A. Bowring[1], Paul J. Umhoefer[2], Robert B. Miller[3], Noah M. McLean[4], and Erin E. Donaghy[2]

[1]*Department of Earth, Atmospheric and Planetary Sciences, Massachusetts Institute of Technology, Cambridge, Massachusetts 02139, USA*

[2]*School of Earth Sciences and Environmental Sustainability, Northern Arizona University, Flagstaff, Arizona 86011, USA*

[3]*Department of Geology, San Jose State University, San Jose, California 95192, USA*

[4]*Department of Geology, University of Kansas, Lawrence, Kansas 66045, USA*

ABSTRACT

The presence of early Eocene near-trench magmatism in western Washington and southern British Columbia has led to speculation that this area experienced ridge-trench interaction during that time. However, the effects of this process as they are preserved in other parts of the geologic record are poorly known. We present high-precision U-Pb zircon geochronology from Paleogene nonmarine sedimentary and volcanic sequences in central and western Washington that preserve a record of tectonic events between ca. 60 and 45 Ma. The data reveal that the Swauk, Chuckanut, and Manastash Formations formed a nonmarine sedimentary basin along the North American margin between ≤59.9 and 51.3 Ma. This basin experienced significant disruption that culminated in basinwide deformation, uplift, and partial erosion during accretion of the Siletzia terrane between 51.3 and 49.9 Ma. Immediately following accretion, dextral strike-slip faulting began, or accelerated, on the Darrington–Devil's Mountain, Entiat, Leavenworth, Eagle Creek, and Straight Creek–Fraser fault zones between 50 and 46 Ma. During this time, the Chumstick Formation was deposited in a strike-slip basin coeval with near-trench magmatism. Faulting continued on the Entiat, Eagle Creek, and Leavenworth faults until a regional sedimentary basin was reestablished ≤45.9 Ma, and may have continued on the Straight Creek–Fraser fault until 35–30 Ma. This record of basin disruption, volcanism, and strike-slip faulting is consistent with ridge-trench interaction and supports the presence of an oceanic spreading ridge at this latitude along the North American margin during the early Eocene.

INTRODUCTION

Ridge-trench interaction is a fundamental tectonic process that can dramatically alter the geology of convergent margins. Such interactions have occurred several times over the past 60 m.y. in western North America as oceanic plates were consumed in E-dipping subduction zones. Most recently (ca. 30 Ma–present), the intersection of the Pacific-Farallon Ridge with the continent has led to the fragmentation of the Farallon plate into multiple microplates (Stock and Lee, 1994), the development of the San Andreas fault (Atwater, 1970), and the generation of geochemically anomalous magmas above slab windows and areas of slab breakoff (e.g., Johnson and O'Neil, 1984; Benoit et al., 2002). Plate reconstructions for the northern Pacific Basin also require subduction of the Kula-Farallon Ridge or Kula-Resurrection and Resurrection-Farallon Ridges along North America's western margin during the early Cenozoic (Fig. 1A; Atwater, 1970; Grow and Atwater, 1970; Wells et al., 1984; Engebretson et al., 1985; Haeussler et al., 2003; Madsen et al., 2006). However, the precise timing and location(s) of this ridge-trench interaction remain uncertain, as the oceanic crust needed to constrain the position of these ridges is completely subducted. Instead, the location of past triple junctions, and consequently the geometry of past plate configurations, must be constrained through the careful identification of the effects of ridge-trench interaction, as they are preserved in the North American geologic record.

Previous studies have identified two areas in the Pacific Northwest that may record Paleogene ridge-trench interaction: the terranes that compose the southern Alaska margin (Fig. 1A) and the Paleogene forearc of southern British Columbia and western Washington. The recognition of these areas has led to several potential plate reconstructions that place oceanic spreading centers intersecting North America along the southern Alaska margin, at the latitude of Washington, or simultaneously in both areas between ca. 60 Ma and 50 Ma (Fig. 1A; Wells et al., 1984; Engebretson et al., 1985; Cowan, 2003; Haeussler et al., 2003; Madsen et al., 2006). Yet, while the effects of ridge-trench interaction are well documented in southern Alaska (Bradley et al., 2003, and references therein), evidence for ridge-trench interaction at the latitude of Washington relies almost exclusively on the existence, and age, of geochemically anomalous near-trench and backarc magmatism (Breitsprecher et al., 2003; Groome et al., 2003; Haeussler et al., 2003; Madsen et al., 2006; Ickert et al., 2009). Ridge-trench interaction has also been invoked, at least in part, to explain the origin and accretion of the oceanic Siletzia terrane to this part of North America during the early Eocene (McCrory and Wilson, 2013; Wells et al., 2014). Nevertheless, few studies have considered other manifestation of Paleogene ridge-trench interaction at this latitude.

In central and western Washington, a series of well-studied Paleogene nonmarine sedimentary and volcanic sequences preserve a record of sedimentation, deformation, and volcanism that may be related to ridge-trench interaction

[†]mpeddy@mit.edu

GSA Bulletin; March/April 2016; v. 128; no. 3/4; p. 425–441; doi: 10.1130/B31335.1; 9 figures; 2 tables; Data Repository item 2015323; published online 28 September 2015.

triple junction migration. However, the tectonic significance of these rocks remains controversial due to disagreements over whether they record sediment accumulation within regional or local basins. Precise geochronology could resolve this issue by temporally correlating these sequences and constraining the age, duration, and spatial extent of tectonic events, and we present 22 high-precision U-Pb zircon dates with this goal in mind. The data reveal an abrupt tectonic change at ca. 50 Ma marked by deformation, bimodal volcanism, and initiation, or significant acceleration, of dextral strike-slip faulting. This change coincides with near-trench magmatism along the Washington and British Columbian coasts (e.g., Madsen et al., 2006), as well as the accretion of the Siletzia terrane to North America (Wells et al., 2014), and we suggest that all of these events are related to triple junction migration.

Figure 1 (*on following page*). (A) Map of the Pacific Northwest that shows possible locations for the Kula-Farallon spreading ridge during the early Paleogene, modified from Haeussler et al. (2003). If the terranes that compose southern Alaska are far-traveled from a more southerly location in the early Paleogene (e.g., Cowan, 2003), the range of possible positions would narrow along the Washington and British Columbia coasts. Alternatively, if the Chugach terrane was not far-traveled, the Resurrection oceanic plate may have existed and would have resulted in two or more ridges intersecting North America (Haeussler et al., 2003; Madsen et al., 2006). (B) Generalized geologic map of central and northwest Washington, including southern Vancouver Island, modified from Walsh et al. (1987), Stoffel et al. (1991), Schuster et al. (1997), Dragovich et al. (2002), and Massey et al. (2005). Paleogene-aged sedimentary formations and regional strike-slip faults discussed in this paper are labeled, and abbreviations are: MH—Mount Higgins area, BP—Barlow Pass area, ECF—Eagle Creek fault, LFZ—Leavenworth fault zone, and DDMFZ—Darrington–Devil's Mountain fault zone. Stars denote the locations of Paleogene-aged adakites, abbreviated: BH—Bremerton Hills, MPV—Mount Persis volcanics, PT—Port Townsend, and peraluminous granites, abbreviated: WCI—Walker Creek intrusions, MPS—Mount Pilchuck suite (Tepper et al., 2004; Madsen et al., 2006; MacDonald et al., 2013). The heavy dashed line marks the inferred boundary between Siletzia and North America (Wells et al., 1998).

PALEOGENE NONMARINE SEDIMENTARY AND VOLCANIC SEQUENCES

Nonmarine sedimentary and volcanic rocks of Paleogene age are exposed as isolated sequences along and between the Straight Creek–Fraser, Darrington–Devil's Mountain, Entiat, and Leavenworth fault zones in central and western Washington (Fig. 1B). They rest unconformably on pre-Tertiary metamorphic basement and are in turn unconformably overlain by Oligocene and younger (33 Ma–present) sedimentary and volcanic rocks. The Paleogene sequences are composed of sandstone, mudstone, and conglomerate deposited in fluvial and lacustrine environments near the Paleogene coastline and are divided into seven formations as well as several informal units. To the west, there are marine sedimentary rocks of approximately the same age in the Puget Group and within the Siletzia terrane (Fig. 1B; Vine, 1969; Buckovic, 1979; Einarsen, 1987; Johnson and O'Connor, 1994), but the precise temporal and depositional relationship between these areas is unknown.

Postdepositional faulting has partly obscured the role that regional strike-slip faults played in the formation of the Paleogene sedimentary sequences discussed in this paper. This uncertainty has resulted in disagreement as to whether they represent distinct basins formed by strike-slip faulting (Johnson, 1985), erosional remnants of a regional depositional system (Cheney, 1994, 2003; Cheney and Hayman, 2009), or a regional system that was later partitioned into distinct strike-slip basins (Evans, 1994). These different models can be tested using a well-constrained correlation scheme. However, while detailed stratigraphic, paleocurrent, and petrologic data are available for each sequence, existing geochronology is too imprecise to make accurate temporal correlations. Despite this difficulty, previous correlation efforts have used a variety of stratigraphic arguments, in addition to existing geochronology, to create regional histories for sedimentation (e.g., Tabor et al., 1984; Cheney, 1994) and fault motion (Gresens et al., 1981; Tabor et al., 1984; Taylor et al., 1988; Evans, 1994; Evans and Ristow, 1994; Cheney, 2003; Cheney and Hayman, 2009). We use our data to test and expand upon these earlier studies.

U-Pb GEOCHRONOLOGY METHODS

We dated 22 samples of volcanic and sedimentary rock from the Paleogene nonmarine sedimentary and volcanic sequences in central and western Washington using U-Pb zircon chemical abrasion–isotope dilution–thermal ionization mass spectrometry (CA-ID-TIMS) geochronology. U-Pb zircon dates represent the age of zircon crystallization and are interpreted as the age of eruption/deposition for volcanic rocks, emplacement for plutonic rocks, or as a maximum depositional age for the youngest detrital zircon grain in sedimentary samples. For detrital analyses, zircons were prescreened using laser-ablation–inductively coupled plasma–mass spectrometry (LA-ICP-MS) at the Arizona LaserChron Center to identify the youngest grains for CA-ID-TIMS analyses. Methods for CA-ID-TIMS are modified from those outlined in Mattinson (2005) and are discussed in more detail in Appendix A. All isotopic ratios were measured on a VG Sector 54 or Isotopx X62 thermal ionization mass spectrometer at Massachusetts Institute of Technology, and the data are presented in Table DR1 and shown as concordia plots in Figure DR1.[1] Our preferred date for each sample is shown in Table 1.

All reported dates represent a weighted mean of ^{238}U-^{206}Pb zircon dates, or a single-grain ^{238}U-^{206}Pb date for samples where taking a weighted mean is inappropriate. A correction for preferential exclusion of ^{230}Th during zircon crystallization was made using a calculated Th/U for each zircon and an assumed magmatic Th/U ratio of 2.8 ± 1 (2σ), which encompasses the range of values seen in most felsic igneous liquids (Machlus et al., 2015). The first time that a date is presented, uncertainty is reported in the format ±*X*/*Y*/*Z*, where *X* is the analytical uncertainty, *Y* is the analytical uncertainty plus the uncertainty in the isotopic composition of the tracer solution, and *Z* also includes the uncertainty in the ^{238}U decay constant. However, since all of the dates reported in this paper were produced using the same isotopic tracer and ^{238}U decay constant, only the analytical uncertainty (2σ) is used in subsequent discussion. For samples where a weighted mean is used, the mean square of weighted deviates (MSWD) is reported, along with the number of grains (*n*) used in the calculation.

Complex zircon populations are common in volcanic rocks, and age dispersion beyond that expected from analytical uncertainty can arise from a variety of sources, including the incorporation of xenocrystic zircon during eruption or deposition and/or protracted zircon crystallization prior to eruption. Some of our volcanic samples contain grains that are >1 m.y. older

[1]GSA Data Repository item 2015323, including isotopic data and concordia plots for each dated sample, is available at http://www.geosociety.org/pubs/ft2015.htm or by request to editing@geosociety.org.

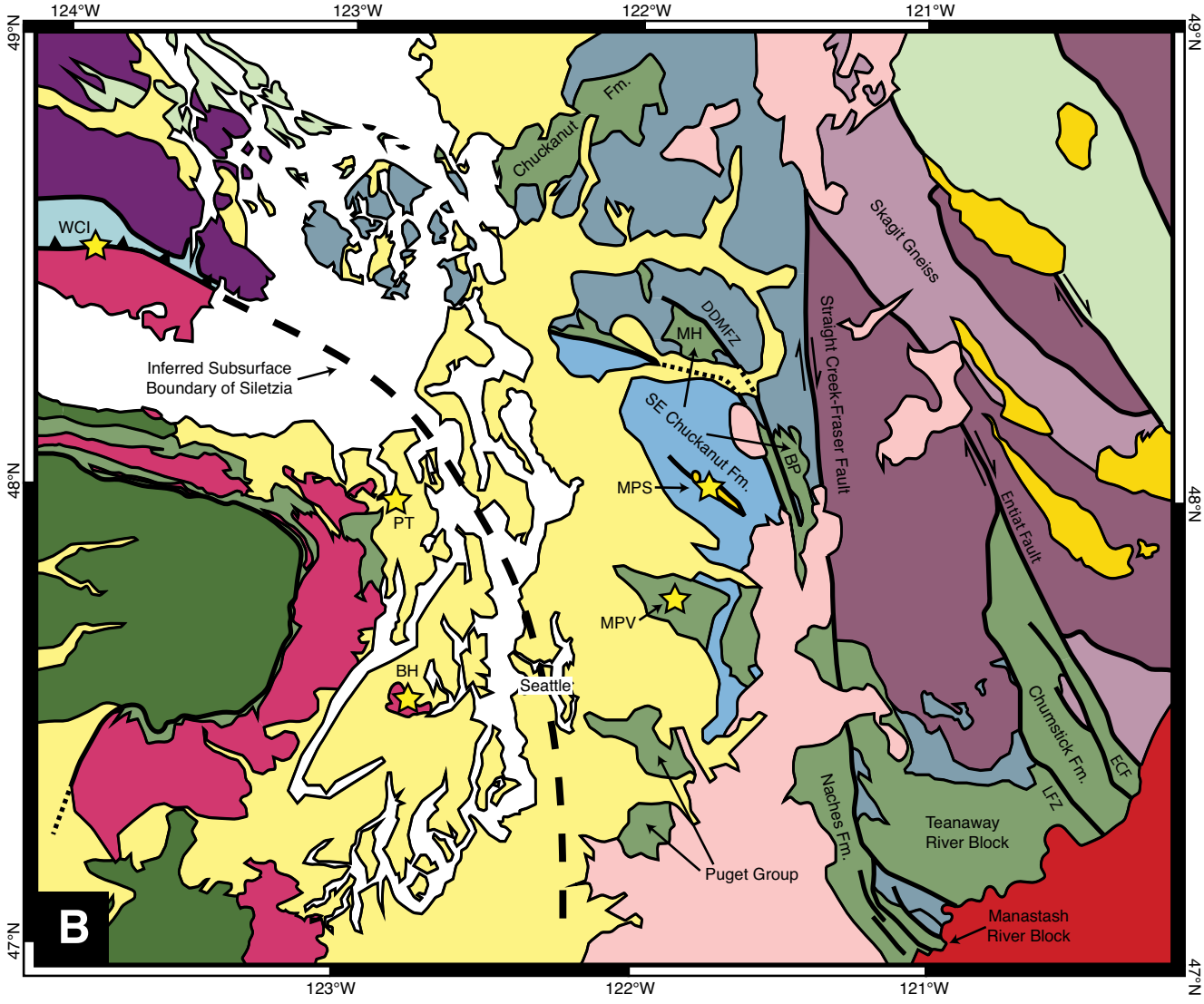
124°W
123°W
122°W
121°W
49°N
48°N
47°N
WCI
Chuckanut Fm.
Skagit Gneiss
DDMFZ
MH
Straight Creek-Fraser Fault
Inferred Subsurface Boundary of Siletzia
SE Chuckanut Fm.
BP
MPS
PT
Entiat Fault
MPV
BH
Seattle
Chumstick Fm.
ECF
LFZ
Naches Fm.
Teanaway River Block
Puget Group
Manastash River Block
B
0 km
50
100
Oligocene to Present
Quaternary alluvium
Columbia River Basalts (ca. 16 Ma)
Sedimentary rock and Quaternary sediment (33 Ma–Present)
Cascade Arc magmatism (40 Ma–Present)
Paleocene and Eocene
Major granitic intrusive complexes (50–46 Ma)
Northern Siletzia (ca. 52–49 Ma)
Sedimentary rock
Ortho- and paragneiss with Eocene cooling ages
Paleogene Adakites and Peraluminous Granites
Faults
Contacts
Mesozoic
Leech River Schist
Western and eastern melange belts
Sedimentary units of the Methow Basin
Northwest Cascades Thrust System
Wrangellia
Ortho- and paragneiss with dominantly Mesozoic cooling ages
A
Southern Alaska Margin
North America
Kula
Range of Possible Ridge Positions
Farallon
Pacific
B

Figure 1.

TABLE 1. CHEMICAL ABRASION–ISOTOPE DILUTION–THERMAL IONIZATION MASS SPECTOMETRY (CA-ID-TIMS) U-Pb ZIRCON DATES

Sample	Lat. (°N)	Long. (°W)	Lithology	Formation, member, or unit	U-Pb zircon CA-ID-TIMS date (Ma)	Interpretation
Lower Swauk basin						
NC-203	48.64150	122.48415	Silicic tuff	Chuckanut Formation	56.835 ± 0.050/0.062/0.087 (n = 6, MSWD = 1.3)	Eruption age
NC-MPE-016	47.44661	121.05611	Sandstone	Basal Swauk Formation	59.919 ± 0.098/0.10/0.12	MDA*
Upper Swauk basin						
NC-190	47.32132	121.18959	Rhyolite	Silver Pass volcanic member	51.364 ± 0.029/0.038/0.067 (n = 6, MSWD = 2.1)	Eruption age
NC-MPE-358B	47.33449	120.63271	Lapilli tuff	Silver Pass volcanic member	51.515 ± 0.028/0.037/0.067 (n = 3, MSWD = 3.0)	Eruption age
NC-MPE-419B	47.06567	120.91241	Rhyolitic tuff	Taneum Formation	51.309 ± 0.024/0.035/0.065 (n = 5, MSWD = 2.1)	Eruption age
Bimodal volcanics						
NC-MPE-420B	48.36277	121.78906	Bentonite	Barlow Pass volcanics	48.999 ± 0.029/0.036/0.063	MDA
NC-MPE-421	48.36696	121.78710	Silicic tuff	Barlow Pass volcanics	49.933 ± 0.059/0.078/0.095 (n = 5, MSWD = 1.9)	Eruption age
NC-MPE-436	47.37613	121.39405	Rhyolite	Naches Formation	49.711 ± 0.024/0.036/0.064 (n = 7, MSWD = 2.1)	Eruption age
NC-MPE-356	47.30607	120.76079	Rhyolite	Teanaway Formation	49.341 ± 0.033/0.046/0.070 (n = 5, MSWD = 2.2)	Eruption age
Chumstick basin						
ED072413-147	47.47495	120.43283	Silicic tuff	Fairview Canyon tuff†	49.147 ± 0.041/0.051/0.073 (n = 6, MSWD = 0.9)	Eruption age
NC-MPE-359	47.52874	120.48180	Silicic tuff	Yaxon Canyon #3 tuff†	48.959 ± 0.037/0.047/0.071 (n = 8, MSWD = 1.3)	Eruption age
ED062313-035	47.63974	120.55926	Silicic tuff	Eagle Creek tuff†	48.522 ± 0.015/0.027/0.058 (n = 6, MSWD = 1.3)	Eruption age
NC-MPE-365B	47.67877	120.60127	Silicic tuff	Clark Canyon #7 tuff†	48.290 ± 0.046/0.054/0.075	MDA
STC62-1	47.33763	120.42613	Silicic tuff	Clark Canyon #4 tuff†	48.186 ± 0.026/0.036/0.063 (n = 5, MSWD = 0.2)	Eruption age
NMNC366-2	47.71413	120.63692	Silicic tuff	Clark Canyon #2 tuff†	47.981 ± 0.019/0.029/0.059 (n = 6, MSWD = 1.1)	Eruption age
ED070113-063	47.62061	120.66200	Sandstone	Clark Canyon Member, Chumstick Formation	47.847 ± 0.085/0.088/0.10	MDA
ED071613-127	47.65514	120.52099	Sandstone	Nahahum Canyon Member, Chumstick Formation	46.902 ± 0.076/0.082/0.096	MDA
Roslyn basin						
NC-MPE-015	47.27604	121.07018	Sandstone	Lower Roslyn Formation	48.80 ± 0.11/0.12/0.13	MDA
NC-MPE-014	47.22681	120.98922	Sandstone	Middle Roslyn Formation	47.580 ± 0.028/0.035/0.062	MDA
NC-MPE-020	47.38746	120.28250	Congl. clast	Deadhorse Canyon Member, Chumstick Formation	45.910 ± 0.021/0.029/0.057 (n = 4, MSWD = 0.7)	MDA
Cascade arc magmatism						
NC-MPE-417A	47.29772	120.82146	Felsic intrusion	Unknown§	25.611 ± 0.014/0.019/0.033 (n = 6, MSWD = 1.6)	Emplacement age
NC-MPE-418	47.33387	120.86729	Rhyolitic tuff	Unknown§	24.216 ± 0.011/0.016/0.030 (n = 3, MSWD = 1.7)	Eruption age

Note: MSWD—mean square of weighted deviates.
*MDA—Maximum depositional age.
†Informal names for tuffs in Clark Canyon Member of the Chumstick Formation established by McClincy (1986).
§These rhyolites were previously considered part of the Teanaway Formation (Clayton, 1973).

than the main population of zircon dates, and we exclude them from our age calculations. Dispersion of zircon dates at the <1 m.y. level is more difficult to evaluate, and we use the MSWD of weighted means to help determine whether this dispersion can be explained by analytical uncertainty (MSWD ≈ 1) or whether it represents resolvable age differences (MSWD >> 1). The range of acceptable MSWD values for different size zircon populations (n) can be calculated using the expected variability of the MSWD (Wendt and Carl, 1991), and we treat samples with MSWD values within the expected 2σ variability as a single population. Samples with age dispersion that cannot be explained by analytical uncertainty are discussed individually in the following sections.

Previous geochronology from these sedimentary sequences was compiled and presented in Tabor et al. (1982, 1984, 1987, 1993, 2000, 2002). These dates were produced using K-Ar or fission-track zircon methods and have associated 2σ uncertainties at the 10%–1% level. Although these dates were invaluable to previous correlation efforts (e.g., Tabor et al., 1984) and largely agree with the U-Pb zircon CA-ID-TIMS dates presented in this paper, their large uncertainties inhibit their use for constraining basin evolution at fine time scales, and they are not discussed further here.

RESULTS

Chuckanut Formation

The Chuckanut Formation is the farthest north of the sedimentary sequences discussed in this paper (Fig. 1B), and it consists of 4000–5000 m of fluvial sandstone, conglomerate, and very rare pyroclastic rock (Fig. 2). Johnson (1984) and Breedlovestrout (2011) described the formation's stratigraphy in detail and provided thickness estimates and sedimentologic data for each of its members. It is interpreted to represent deposits along SW-flowing streams, and Johnson (1984) suggested that it had a distal sediment

source in eastern Washington or Idaho. However, the Governor's Point and Maple Falls Members (Fig. 2) may have been derived from local topographic highs (Johnson, 1984). After deposition, the Chuckanut Formation was deformed into a NW-trending fold belt and eroded, resulting in an angular unconformity between the formation and the overlying Oligocene Huntingdon Formation (Miller and Misch, 1963; Johnson, 1984).

A date for a tuff (NC-203) collected from the lower Bellingham Bay Member (Fig. 2) provides a temporal constraint on the beginning of sediment accumulation in the Chuckanut Formation. Individual zircons from this sample have dates that span 870 k.y. and exceed the dispersion expected from analytical uncertainty (MSWD = 6.5 for all 16 grains). The date for the youngest zircon overlaps with the next five youngest grains within 2σ uncertainty, and a weighted mean of these grains gives our preferred eruption/depositional age of 56.835 ± 0.050/0.062/0.087 Ma (n = 6, MSWD = 1.3), demonstrating that sediment accumulation began in the Chuckanut Formation prior to this date (Fig. 2). Other high-precision dates from this formation were reported in Breedlovestrout et al. (2013) and include a tuff that is interbedded within the upper Slide Member (Fig. 2) and a rhyolitic dike that intrudes the lower Padden Member. Zircons from the tuff gave a weighted mean date of 53.676 ± 0.023/0.035/0.067 Ma and provide a constraint on the age of the middle Chuckanut Formation, whereas zircons from the dike gave a weighted mean date of 49.858 ± 0.025/0.035/0.063 Ma. To our knowledge, this is the only dike reported within the Chuckanut Formation, and its significance in relation to regional magmatism remains uncertain. Nevertheless, its intrusive relationship with the Padden Member requires the member to have been deposited prior to 49.858 ± 0.025 Ma.

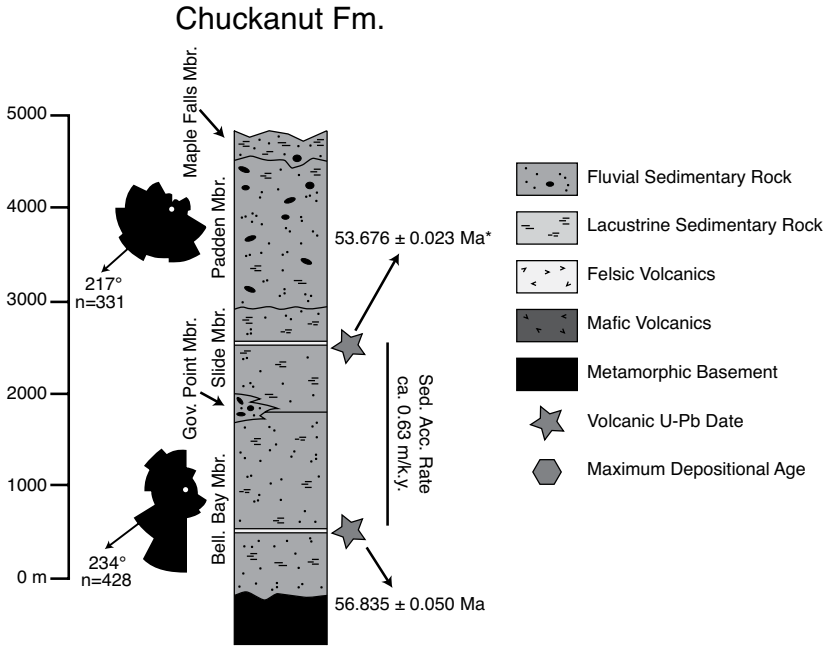

Figure 2. Generalized stratigraphic column of the Chuckanut Formation. Member thicknesses and paleocurrent data are from Breedlovestrout (2011) and Johnson (1985). All dates are U-Pb zircon chemical abrasion–isotope dilution–thermal ionization mass spectrometry (CA-ID-TIMS) dates reported in this paper, with the exception of the date denoted with an asterisk, which was previously reported in Breedlovestrout et al. (2013). Sediment accumulation (Sed. Acc.) rates are assumed to be linear.

Southeastern Chuckanut Formation

To the SE of the main outcrop belt of the Chuckanut Formation, there lie thick packages of sedimentary and volcanic rock that are cut by splays of the Darrington–Devil's Mountain fault zone (Fig. 1B). Evans and Ristow (1994) called these rocks the SE Chuckanut Formation and described two detailed stratigraphic sections. The first is exposed in the area around Mount Higgins (Fig. 1B) and was informally split into the Coal Mountain and Higgins Mountain units based on a reversal in paleocurrent direction from SW to NE. The Coal Mountain unit records SW-directed paleoflow and consists of 2250 m of sandstone with minor shale, coal, and conglomerate (Fig. 3). It is conformably overlain by the Higgins Mountain unit, which con-

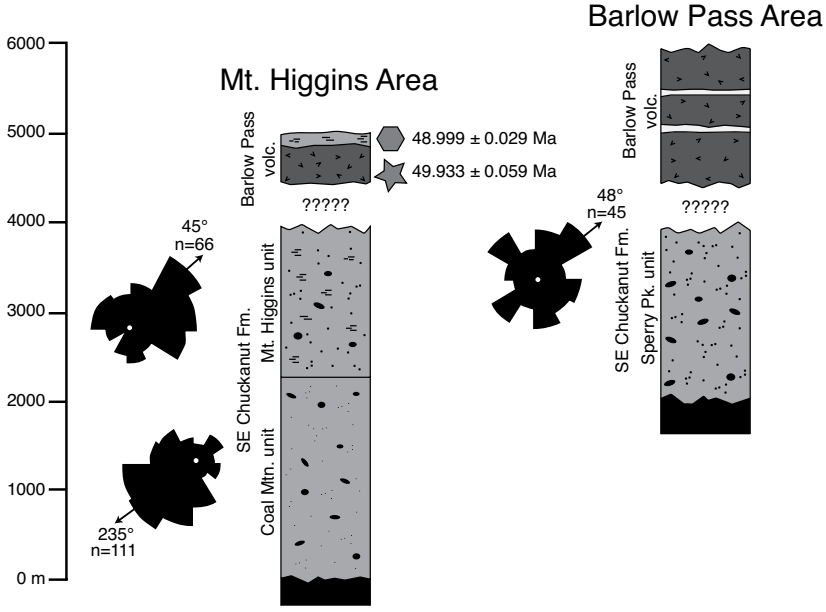

Figure 3. Generalized stratigraphic column of the SE Chuckanut Formation. Unit thicknesses and paleocurrent data are from Evans and Ristow (1994). All dates are U-Pb zircon chemical abrasion–isotope dilution–thermal ionization mass spectrometry (CA-ID-TIMS) dates reported in this paper, and the columns are hung so that correlative sedimentary units are adjacent to one another. Symbols are the same as Figure 2.

sists of 1700 m of sandstone, shale, and minor conglomerate that record NE-directed paleoflow (Fig. 3). Conglomerate clasts within the Higgins Mountain unit are dominantly quartz, phyllite, tuff, and chert (Evans and Ristow, 1994). These lithologies are common in the western and eastern mélange belts (Fig. 1B), and their presence within the Higgins Mountain unit, along with the unit's NE-directed paleoflow, suggests that the mélange belts were uplifted and eroding during its deposition. Evans and Ristow (1994) described an unconformable contact between the Higgins Mountain unit and the overlying rhyolite and andesite flows of the Barlow Pass volcanics (Fig. 3). However, angular discordance in this area is slight, and Tabor (1994) and Tabor et al. (1993, 2002) did not consider the unconformity to be significant.

Zircons separated from a rhyolitic tuff (NC-MPE-421) at the base of the Barlow Pass volcanics in the Higgins Mountain area (Fig. 3) have dates that span 460 k.y. and exceed the age dispersion expected from analytical uncertainty. The youngest five grains overlap within 2σ uncertainty and give a weighted mean date of 49.933 ± 0.059/0.078/0.095 Ma (n = 5, MSWD = 1.9). This date constrains the initiation of Barlow Pass volcanism and demonstrates that both the Higgins Mountain and Coal Mountain units are older than 49.933 ± 0.059 Ma. A bentonite (NC-MPE-420B) interbedded with a sequence of black shale was also collected from this area. Zircons from this sample do not form a single population of dates within analytical uncertainty, and therefore we treat the date of the youngest grain, 48.999 ± 0.029/0.036/0.063 Ma, as a maximum depositional age. Cruver (1981), Evans and Ristow (1994), and Dragovich et al. (2003) all considered this sequence to belong to Higgins Mountain unit. However, our maximum depositional age shows that they are younger than the basal Barlow Pass volcanics (Fig. 3). This date is consistent with mapping by Tabor et al. (2002) that showed that these rocks overlie the Barlow Pass volcanics, and we therefore consider this small sedimentary section to be distinct from the Higgins Mountain unit.

In the area around Barlow Pass, Evans and Ristow (1994) measured 1900 m of steeply dipping sedimentary rock that they informally named the Sperry Peak unit (Fig. 3). This unit unconformably overlies metamorphic bedrock and consists of sandstone and shale that record NE-directed paleoflow, as well as conglomerate with a high percentage of chert clasts. Like the Higgins Mountain unit, the NE paleoflow and high percentage of chert clasts in the Sperry Peak unit suggest a sediment source in the western and eastern mélange belts, and these features provide circumstantial evidence for the correlation of these two units (Evans and Ristow, 1994). Overlying the Sperry Peak unit, >1200 m of basalt and minor rhyolite form part of the Barlow Pass volcanics (Fig. 3). The volcanics dip gently to the east, and Vance (1957) and Evans and Ristow (1994) considered them to unconformably overlie the Sperry Peak unit based on their contrasting degree of deformation. However, the Barlow Pass volcanics and Sperry Peak unit are only seen in fault contact, and Tabor et al. (2002) suggested that this difference might represent proximity to active structures or a difference in mechanical properties rather than an angular unconformity.

None of our samples from the Barlow Pass area yielded zircon. Nevertheless, we follow Evans and Ristow (1994) and consider the Sperry Peak and Higgins Mountain units to be correlative based on their overall sedimentological similarities. It is important to note that Tabor et al. (1993, 2002) considered the Coal Mountain, Higgins Mountain, and Sperry Peak units to be a sedimentary facies of the Barlow Pass volcanics. These authors emphasized the presence of abundant tuffs in the sedimentary rock near Mount Higgins (e.g., Cruver, 1981) and did not consider the unconformity between the SE Chuckanut Formation and the overlying volcanics to be significant. Our geochronologic data show that the tuff-bearing rocks described by Cruver (1981) are younger than the SE Chuckanut Formation as described by Evans and Ristow (1994), and, like these authors, we consider the SE Chuckanut Formation and the Barlow Pass volcanics to be distinct.

Naches Formation

The Naches Formation is a sequence of basalt and rhyolite flows interbedded with nonmarine sedimentary rock exposed near the presumed southern termination of the Straight Creek–Fraser fault (Fig. 1B). An accurate thickness is difficult to obtain due to a lack of marker beds and complex folding and faulting, but Tabor et al. (1984) estimated a total thickness between 1500 and 3000 m (Fig. 4). The nonmarine sedimentary rocks that constitute the lower Naches Formation are named the Guye Member and are interbedded with rhyolite flows of the Mount Catherine rhyolite (Tabor et al., 1984). A sample collected from the Mount Catherine rhyolite near the top of the Guye Member gives a U-Pb zircon date of 49.711 ± 0.024/0.036/0.064 Ma (n = 7, MSWD = 2.1) and provides a minimum age for the underlying sedimentary rocks as well as a maximum age for the ~1500 m of basalt, andesite, and rhyolite that form the upper Naches Formation (Fig. 4). Interestingly, the sandstones and conglomerates in the Guye Member are rich in chert (Foster, 1960) and may represent the same period of W-derived sedimentation as the Higgins Mountain and Sperry Peak units.

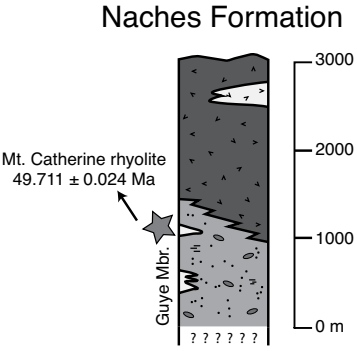

Figure 4. Generalized stratigraphic column of the Naches Formation. Thicknesses are based on Tabor et al. (1984, 2000). The date is a U-Pb zircon chemical abrasion–isotope dilution–thermal ionization mass spectrometry (CA-ID-TIMS) date reported in this paper. Symbols are the same as Figure 2.

Manastash River Block

The Manastash River block of Tabor et al. (1984) consists of an ~1750–2250 m section of sedimentary and volcanic rock exposed between two splays of the southern Straight Creek–Fraser fault (Fig. 1B). The oldest formation exposed in this sequence is the Manastash Formation, and it consists of 500–750 m of arkosic sandstone and minor shale, conglomerate, and coal unconformably deposited on pre-Tertiary bedrock (Fig. 5; Tabor et al., 1984, 2000). The Manastash Formation is in turn overlain by 1000 m of andesitic to rhyolitic flows named the Taneum Formation (Fig. 5). A sample of a rhyolitic tuff (NC-MPE-419B) collected from the Taneum Formation yielded a youngest population of five zircons that give a date of 51.309 ± 0.024/0.035/0.065 Ma (n = 5, MSWD = 2.1), which places a minimum age constraint on the underlying Manastash Formation. Overlying the Taneum Formation with an ambiguous contact, there is the 250–500-m-thick Basalt of Frost Mountain (Fig. 5). Tabor et al. (1984) suggested that there was an unconformity between these two volcanic sequences. However, it is difficult to evaluate this relationship because there is little to no angular discordance between them.

Teanaway River Block

The Teanaway River block (Tabor et al., 1984) consists of three sedimentary and volcanic formations of Paleogene age that lie between the

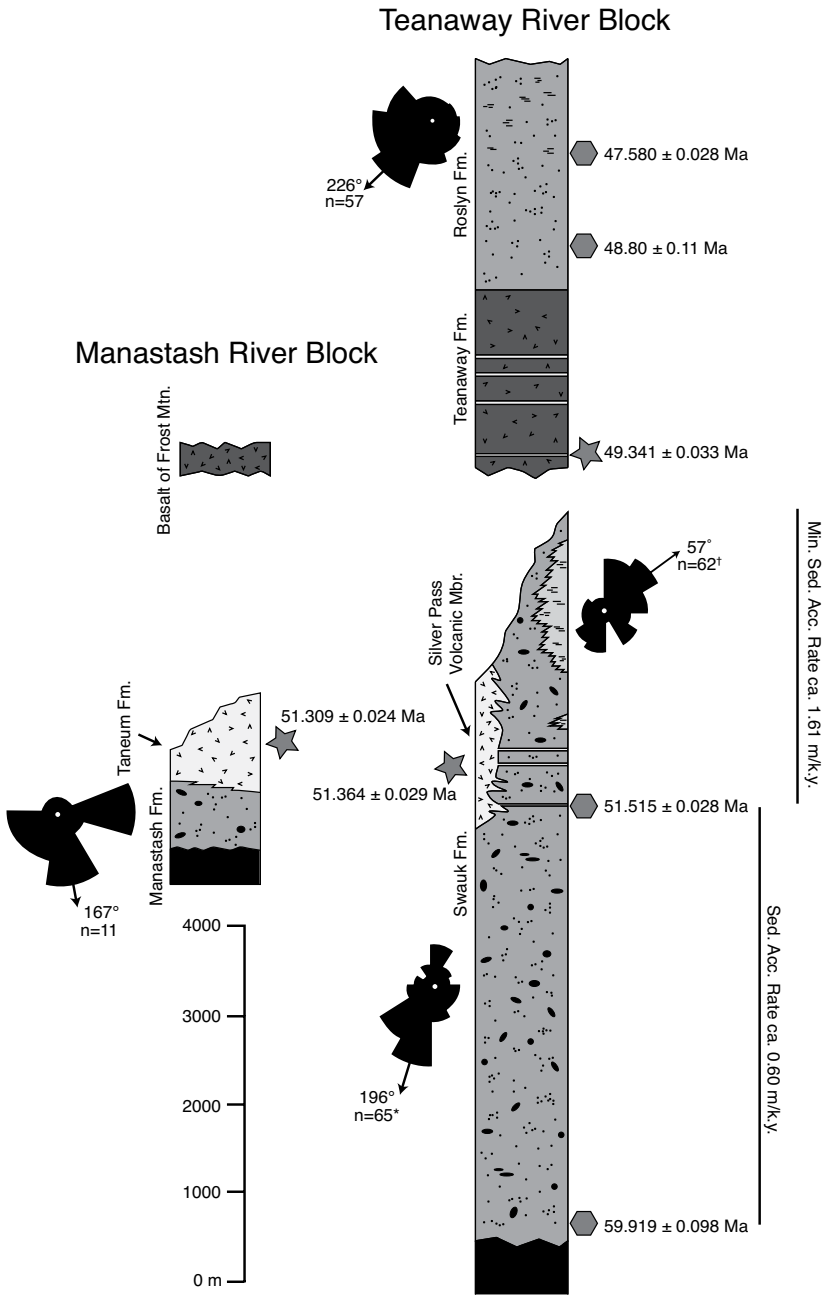

Figure 5. Generalized stratigraphic column of sedimentary and volcanic rocks preserved in the Manastash River and Teanaway River blocks. Thicknesses are from Clayton (1973), Tabor et al. (1982, 1984, 2000), and Taylor et al. (1988), and paleocurrent data are from Barnett (1985), Johnson (1985), and Taylor et al. (1988). The rose diagrams for the lower and upper Swauk Formation represent measurements from the sandstone of Swauk Pass (*) and shale facies of Tronson Ridge (†), respectively. All dates represent U-Pb zircon chemical abrasion–isotope dilution–thermal ionization mass spectrometry (CA-ID-TIMS) dates presented in this paper, and the columns are hung so that correlative sedimentary and volcanic formations are adjacent to one another. Symbols are the same as Figure 2, and sediment accumulation (Sed. Acc.) rates are assumed to be linear.

Straight Creek–Fraser and Leavenworth fault zones (Fig. 1B). The Swauk Formation is the oldest formation in this sequence and is composed of fluvial and lacustrine sedimentary rocks that unconformably overlie pre-Tertiary bedrock (Fig. 5). The total thickness of the formation is difficult to determine due to a lack of marker beds, pervasive intrusion of basaltic dikes, and postdepositional shortening. However, Tabor et al. (2000) estimated that it could be as thick as 8000 m based on combined sections from the eastern and western parts of its outcrop area. The western part of the Swauk Formation remains poorly studied, whereas Taylor et al. (1988) described the upper 4000 m of the eastern part of the Swauk Formation in detail. The lower portion of their section is dominated by arkosic sandstones and rare tuff interpreted to have been deposited in a low-energy fluvial environment with paleoflow to the SSW, and the upper ~2000 m section is composed of conglomerate, shale, and sandstone that largely record paleoflow to the NE (Fig. 5). Taylor et al. (1988) correlated the tuffs in their study area to the Silver Pass Member, which consists of 1800 m of andesitic and rhyolitic flows interbedded with the western part of the Swauk Formation. However, this correlation has never been tested using high-precision geochronology.

We produced three U-Pb zircon dates from the Swauk Formation. A detrital zircon from a sandstone (NC-MPE-016) collected <10 m above the base of the formation gives a maximum depositional age of 59.919 ± 0.098/0.10/0.12 Ma (Fig. 5). Two samples of the Silver Pass volcanic member were also dated (Fig. 5). The first is a rhyolite (NC-190) collected from the type area for the Silver Pass Member in the western Swauk Formation. It contains zircons that have ages that span 971 k.y. and greatly exceed the age dispersion expected from analytical uncertainty (MSWD = 50 for all 11 grains). The youngest grain overlaps within 2σ uncertainty with the next five youngest grains, and they collectively give a weighted mean date of 51.364 ± 0.029/0.038/0.067 Ma (n = 6, MSWD = 2.1). A tuff (NC-MPE-358B) collected ~3000 m below the top of the formation in the eastern part of the Swauk Formation contains abundant detrital zircon ranging in age from 90 to 52 Ma. Nevertheless, the three youngest zircons form a distinct population with a weighted mean date of 51.515 ± 0.028/0.037/0.067 Ma (n = 3, MSWD = 3.0), which we interpret as an eruption/deposition age. The similarity between the ages of NC-MPE-358B and NC-190 confirms a temporal correlation between the tuffs in the eastern Swauk Formation and the Silver Pass volcanic member in the western Sauk Formation and therefore supports Tabor et al.'s (2000) thickness estimate of ~8000 m for the formation as a whole.

The Swauk Formation was shortened into a W-NW–trending fold belt (Doran, 2009), eroded, and unconformably overlain by 800–1200 m of basaltic flows and tuffs, and minor rhyolites and fluvial sedimentary rocks named the Teanaway Formation (Fig. 5; Clayton, 1973). The five youngest zircons from a rhyolite (NC-MPE-456) sampled ~200 m above the base of the Teanaway Formation give a weighted mean date of 49.341 ± 0.033/0.046/0.070 Ma (n = 5, MSWD = 2.2) and tightly constrain the period of shortening recorded by the Swauk Formation to between 51.364 ± 0.029 and 49.341 ± 0.033 Ma (Fig. 5). This date also provides our best estimate for the age of a NE-striking swarm of basaltic dikes that intrude the Swauk Formation and likely fed the overlying basalt flows in the Teanaway Formation (Clayton, 1973; Doran, 2009). In an attempt to date the upper Teanaway Formation, two samples of rhyolite were collected from isolated outcrops with uncertain field relationships near the formation's contact with the overlying Roslyn Formation. Clayton (1973) considered these rhyolites to be part of the Teanaway Formation, but subsequent geochronology reported by Tabor et al. (1982) suggested that they might be considerably younger. Our dates of 25.611 ± 0.014/0.019/0.033 Ma (n = 6, MSWD = 1.6) from a shallow rhyolite intrusion (NC-MPE-417A) and 24.216 ± 0.011/0.016/0.030 Ma (n = 3, MSWD = 1.7) from a poorly exposed rhyolitic tuff (NC-MPE-418) confirm the geochronology by Tabor et al. (1982) and demonstrate that these rhyolites are much younger than the Paleogene sequences discussed in this paper.

Conformably overlying the Teanaway Formation, there is an ~2500 m section of nonmarine arkosic sandstone named the Roslyn Formation, which contains abundant coal seams and was deposited along W-flowing streams (Fig. 5; Walker, 1980; Tabor et al., 1984; Barnett, 1985). Cheney and Hayman (2009) correlated this formation to the Chumstick Formation based on their similar lithologies and paleocurrent direction, but this correlation remains controversial and untested with high-precision geochronology. Two maximum depositional ages of 48.80 ± 0.11/0.12/0.13 Ma from the lower (NC-MPE-015) and 47.580 ± 0.028/0.035/0.062 Ma from the upper (NC-MPE-014) Roslyn Formation will be used to further evaluate this correlation.

Chumstick Formation

The Chumstick Formation is exposed between the Leavenworth and Entiat fault zones (Fig. 1B), and the formation's thickness, stratigraphy, and relationship to these fault systems remain controversial. Johnson (1985, 1996) interpreted the formation as a strike-slip basin, while Evans (1994, 1996) concluded that only part of it was deposited during strike-slip faulting. More recently, Cheney and Hayman (2009) correlated it to the Roslyn Formation across the Leavenworth fault zone and rejected syndepositional strike-slip faulting. Therefore, different interpretations of this formation can result in dramatically different histories for regional strike-slip faulting. Given its importance, we produced nine U-Pb zircon dates that help to resolve these issues.

Gresens et al. (1981) and Evans (1994) presented the most detailed studies of the Chumstick Formation, recognized that the Eagle Creek fault (Fig. 1B) divides it into two sedimentary sections, and established its most widely used stratigraphic nomenclature. The thickness of each section was given by Evans (1994) and is 12,800 m to the west and 4100 m to the east of the Eagle Creek fault. Both of these sections are extremely thick, and previous geochronology suggested rapid accumulation (Evans, 1994). However, Cheney and Hayman (2009) suggested that these thicknesses were overstated and gave a more conservative thickness of ~5200 m for the Chumstick Formation based on their mapping.

The oldest member of the Chumstick Formation is named the Clark Canyon Member, and it consists of sandstone, mudstones, and conglomerate deposited by W-flowing streams (Fig. 6; Evans, 1994). It is currently exposed between the Eagle Creek and Leavenworth fault zones, but its original extent is debated (Evans, 1994; Johnson, 1996; Cheney and Hayman, 2009). McClincy (1986) and Evans (1994) used 18 interbedded tuffs as marker beds and estimated a total thickness of 10,600 m for this member, but Cheney and Hayman (2009) disputed whether these tuffs were traceable over long distances and suggested that the member is substantially thinner. In order to check the validity of the stratigraphy by McClincy (1986) and Evans (1994), we produced six dates from tuffs interbedded with the lower, middle, and upper parts of the Clark Canyon Member and one maximum depositional age from a sample of sandstone collected from the upper Clark Canyon Member

Zircons from the stratigraphically lowest sample (Fairview Canyon tuff; ED072413–147) give a date of 49.147 ± 0.041/0.051/0.073 Ma (n = 6, MSWD = 0.9) and constrain the age of initial sediment accumulation within the Chumstick Formation (Fig. 6). Five additional tuffs were dated from stratigraphic positions above the Fairview Canyon tuff, and the resulting dates are presented in Table 1 and shown on Figure 6. All of these samples, with the exception of the Clark Canyon #7 tuff, contained a single population of zircon dates and are interpreted to represent the age of eruption/deposition. The Clark Canyon #7 tuff (NC-MPE-365B) contained a mixed population of zircon dates, and we take the conservative approach of using the youngest grain as a maximum depositional age. A sample of sandstone collected from ~300 m above the Clark Canyon #2 tuff (Fig. 6) contained a zircon with a date of 47.847 ± 0.085/0.088/0.10 Ma, and this provides a maximum depositional age for the uppermost part of Clark Canyon Member. Notably, all of the dates agree with the stratigraphy proposed by McClincy (1986) and Evans (1994), support their thickness estimates, and confirm rapid sediment accumulation rates of ~6–7 m/k.y. within the lower and middle Clark Canyon Member, and ~2–3.3 m/k.y. in the upper Clark Canyon Member (Fig. 6).

The Tumwater Mountain Member of the Chumstick Formation is interbedded with the Clark Canyon Member along the Leavenworth fault zone and is composed of conglomerate, sandstone, and mudstones for which facies distribution, paleocurrent indicators, and distinctive clast lithologies suggest a proximal sediment source across the fault zone (Evans, 1994). Evidence for syndepositional faulting on the Leavenworth fault zone comes from soft-sediment deformation that is compatible with paleoearthquake activity (Evans, 1994) and extremely coarse conglomerates (clasts >1 m in diameter) near the southern end of the member that are monolithologic and separated by >30 km along the Leavenworth fault zone from their distinctive source areas (Gresens et al., 1981; Evans, 1994). The precise age of this member is poorly constrained, but it is interbedded with rocks of the Clark Canyon Member and therefore must have been deposited between ca. 49 and 47 Ma.

The Nahahum Canyon Member is the stratigraphically lowest member of the Chumstick Formation exposed to the east of the Eagle Creek fault. Evans (1994) considered it to be younger than the Clark Canyon Member, since it lacks interbedded tuffs, it represents disruption of the W-directed drainage system that fed the Clark Canyon Member, and it contains distinctive lacustrine sequences. The member has a minimum thickness of 1900 m (Fig. 6), and Evans (1994) interpreted it as a strike-slip basin between the Eagle Creek and Entiat fault systems. There is abundant sedimentologic data to support this interpretation, including coarse-grained facies adjacent to the member's bounding faults, basin-axial paleoflow, and soft-sediment deformation compatible with syndepositional earthquake activity (Evans, 1994). A detrital zircon from sandstone (ED071613–127)

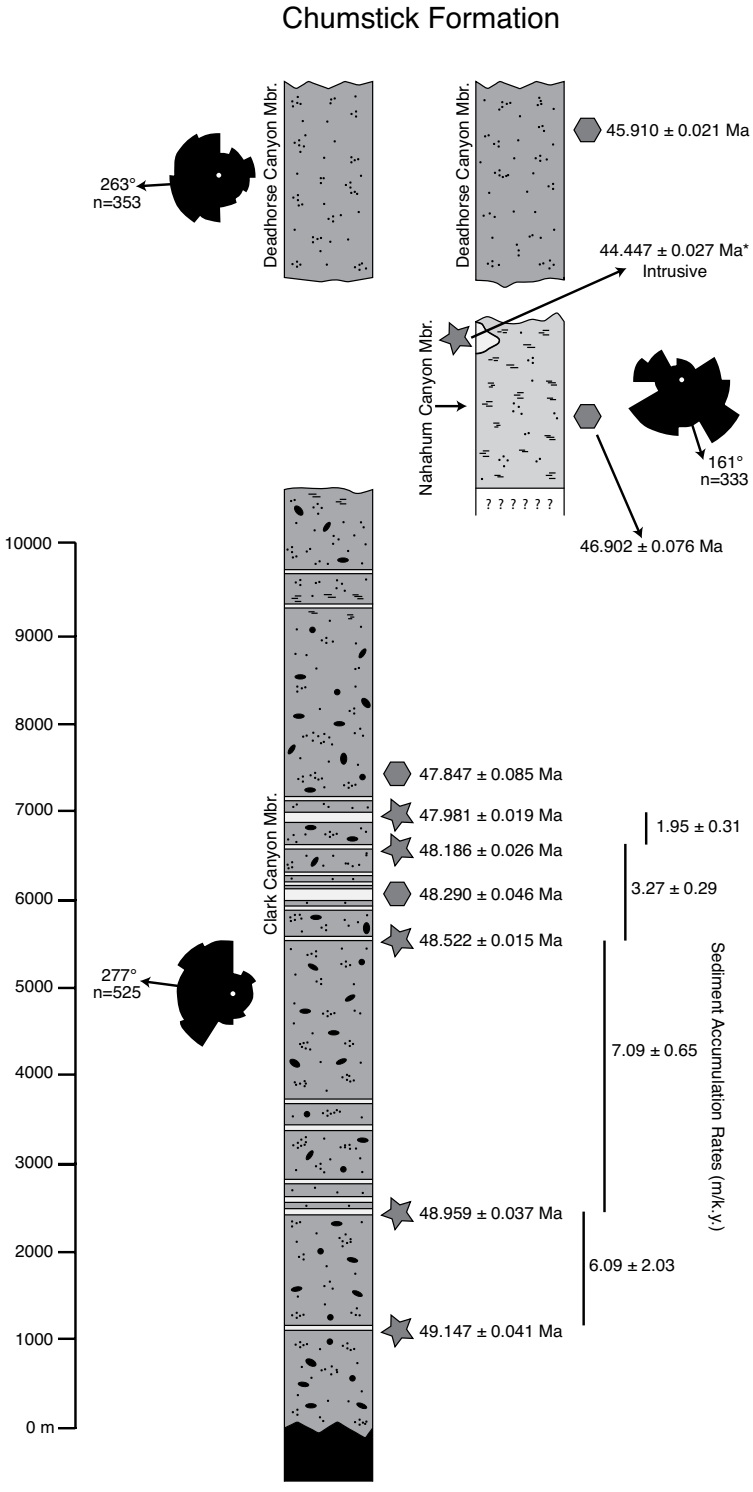

Figure 6. Generalized stratigraphic column from the Chumstick Formation. The Tumwater Mountain Member is not shown, but it is interbedded with the Clark Canyon Member along the Leavenworth fault zone. Thicknesses and paleocurrent data are from Evans (1994), and all dates represent U-Pb zircon chemical abrasion–isotope dilution–thermal ionization mass spectrometry (CA-ID-TIMS) dates presented in this paper, with the exception of the date denoted with an asterisk, which was previously reported by Gilmour (2012). Columns are hung so that correlative members are adjacent to one another. Symbols are the same as Figure 2, and sediment accumulation rates are assumed to be linear.

in the middle of the Nahahum Canyon Member gives a maximum depositional age of 46.902 ± 0.076/0.082/0.096 Ma, and a minimum age for major displacement on the Eagle Creek fault is provided by a U-Pb zircon date of 44.447 ± 0.027/0.035/0.059 Ma from a shallow rhyodacite intrusion that seals this structure (Gilmour, 2012).

The 2200-m-thick Deadhorse Canyon Member was described by Evans (1994) and unconformably overlies both the eastern and western sections of the Chumstick Formation (Fig. 6). This member records W-directed paleoflow and contains no evidence for a syndepositional relationship with adjacent fault zones. Indeed, small outcrops of this member are present on both sides of the Eagle Creek and Entiat fault zones and preclude major strike-slip motion on these structures after its deposition. Zircons from a clast of flow-banded rhyolite collected from the Deadhorse Canyon Member (NC-MPE-020) give a date of 45.910 ± 0.021/0.029/0.057 Ma (n = 4, MSWD = 0.7) and provide a maximum depositional age for this member.

Our nine new U-Pb dates from the Chumstick Formation directly bear on the correlation of these rocks with the formations in the adjacent Teanaway River block. The 49.147 ± 0.041 Ma date for the Fairview Canyon tuff near the base of the Clark Canyon Member demonstrates that sediment accumulation in the Chumstick Formation initiated during eruption of the lower Teanaway Formation and that it is younger than the adjacent Swauk Formation. Our maximum depositional ages of 48.80 ± 0.11 Ma and 47.580 ± 0.028 Ma for the lower and middle Roslyn Formation make it possible that this formation is, in part, correlative with the Chumstick Formation (Cheney, 2003; Cheney and Hayman, 2009). However, we think that the Roslyn Formation is distinctly younger than most of the Chumstick Formation because (1) the Roslyn Formation does not contain abundant tuffs, (2) there is substantial evidence for uplift along the Leavenworth fault preserved in the Tumwater Mountain Member of the Chumstick Formation, precluding a continuous depositional system across this structure until after ca. 47 Ma, and (3) the Roslyn Formation contains no evidence for syndepositional strike-slip faulting. Instead, we consider the Clark Canyon, Tumwater Mountain, and Nahahum Canyon Members of the Chumstick Formation to represent a distinct sedimentary package that was deposited during strike-slip faulting starting slightly before 49.147 ± 0.041 Ma and ending prior to 44.447 ± 0.027 Ma (Table 2), and we interpret the Deadhorse Canyon Member and Roslyn Formation to represent a continuous depositional system that is younger than 45.910 ± 0.021 Ma (Table 2).

TABLE 2. REGIONAL CORRELATIONS

Unit name	Age	Included sedimentary sequences	Description
Renewed regional depositional system			
Roslyn basin	≤45.9 Ma	Deadhorse Canyon Member of the Chumstick Formation, Roslyn Formation	Sandstones, mudstones, and coal that overtop major structures and record sedimentation along meandering rivers that flowed east to west.
Sedimentation during strike-slip faulting			
Chumstick basin	49 to ca. 46 Ma	Clark Canyon Member, Nahahum Canyon Member, and Tumwater Canyon Member of the Chumstick Formation	Sandstones, conglomerates, and mudstones that record extremely high sediment accumulation rates (up to 7 m/k.y.), and have evidence for syndepositional faulting.
Bimodal volcanism			
No regional name	49.9 Ma to ???	Upper Naches Formation, Barlow Pass volcanics, Basalt of Frost Mountain, Teanaway Formation	Dominantly basaltic flows with interbedded rhyolites and fluvial sedimentary rock.
Swauk basin			
Upper Swauk basin	51.3 to >49.9 Ma	Higgins Mountain unit of the SE Chuckanut Formation, Sperry Peak unit of the SE Chuckanut Formation, Swauk Formation above Silver Pass Member, possibly the Guye Member of the Naches Formation	Sandstones, conglomerates, and mudstones that dominantly record E- or NE-directed paleoflow and contain conglomerate clasts likely sourced from the western and eastern mélange belts.
Silver Pass volcanics	ca. 51.5–51 Ma	Taneum Formation, Silver Pass volcanic member	Andesitic to rhyolitic volcanic rocks of unknown tectonic setting.
Lower Swauk basin	≤59.9 to 51.3 Ma	Swauk Formation below Silver Pass Member, Manastash Formation, Coal Mountain unit of the SE Chuckanut Formation, Chuckanut Formation	Sandstones, conglomerates, and mudstones deposited along SW-flowing rivers.

STRATIGRAPHIC CORRELATIONS AND BASIN EVOLUTION

Swauk Basin

Restoration of 100–150 km of dextral motion on the Straight Creek–Fraser fault (e.g., Umhoefer and Miller, 1996) places the Chuckanut and Swauk Formations adjacent to one another (Fig. 7) and has long led to speculation that they accumulated within a single depositional system (e.g., Frizzell, 1979). The U-Pb zircon geochronology presented in this paper confirms that both of these formations, along with the Manastash Formation, were deposited during the same period of time between ≤59.9 and >49.9 Ma (Fig. 8). Paleocurrent indicators suggest that sediment accumulation occurred along W- or SW-flowing streams between ≤59.9 and 51.3 Ma, followed by a reversal in paleoflow direction to the NE between 51.3 and >49.9 Ma (Fig. 7). Sediment accumulation ended before 49.9 Ma (Fig. 8) and was marked by NNE-SSW–directed shortening and basin inversion. Given that these formations record similar patterns of paleoflow, were deposited over the same period of time, and restore adjacent to one another across the Straight Creek–Fraser fault, we believe that they represent erosional remnants of a single depositional system that we call the Swauk basin. Our preferred correlation scheme for rocks within the Swauk basin is shown in Table 2. Most of these correlations are not new and have been previously discussed at both the local and regional levels (e.g., Frizzell, 1979; Tabor et al., 1984; Cheney, 1994, 2003;

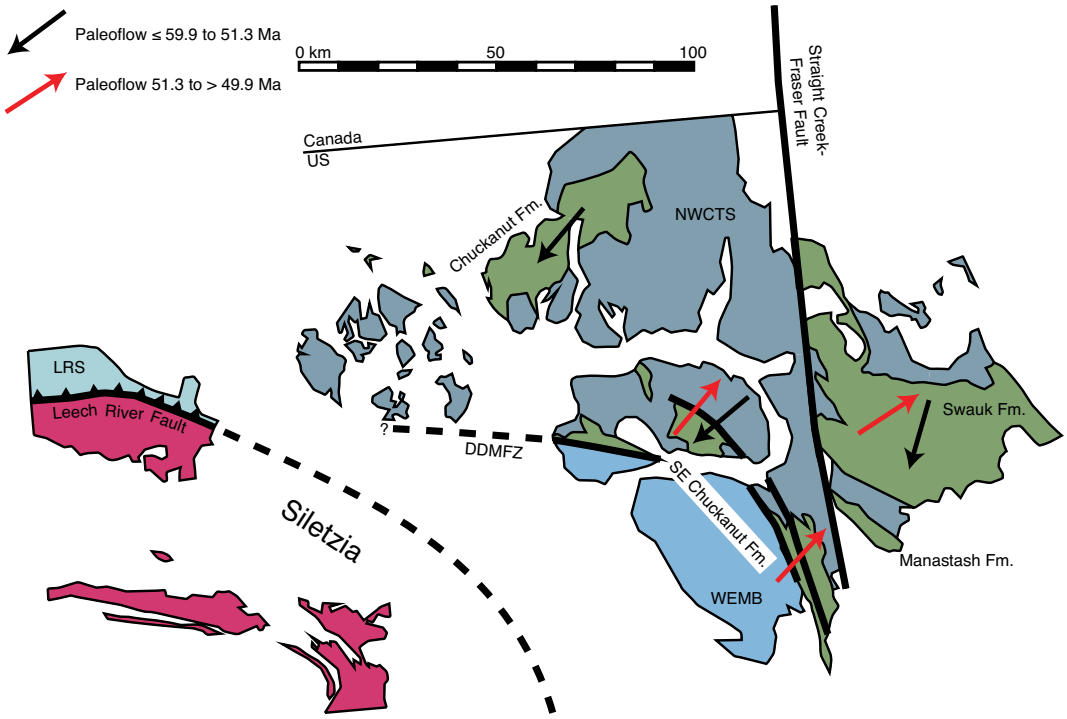

Figure 7. Map showing the relative positions of the formations that compose the Swauk basin with restoration of 125 km of dextral offset on the Straight Creek–Fraser fault. The positions of the Northwest Cascades thrust system (NWCTS), western and eastern mélange belts (WEMB), Leech River Schist (LRS), and Siletzia are also shown. DDMFZ—Darrington–Devil's Mountain fault zone.

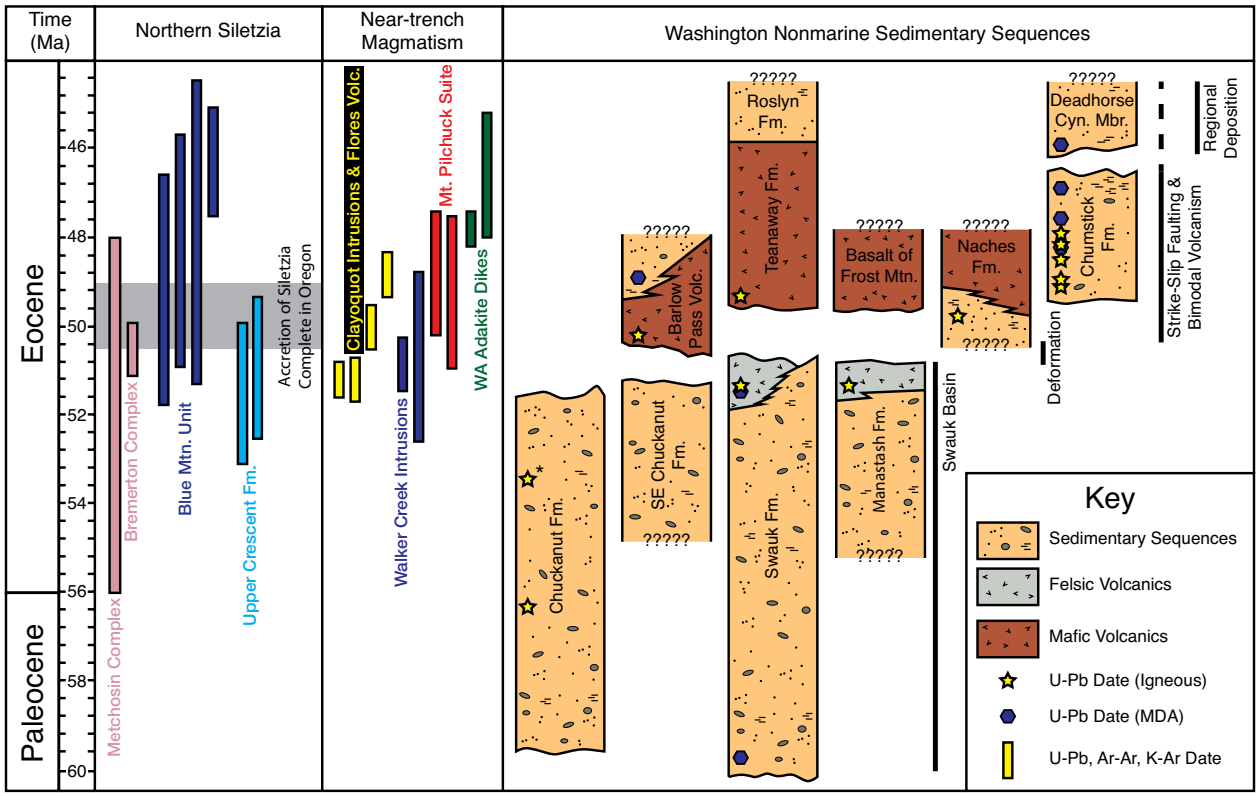

Figure 8. Temporal evolution of the sedimentary sequences discussed in this paper compared to available geochronology from northern Siletzia and near-trench magmatism in western Washington and southern Vancouver Island. All geochronology is shown with 2σ uncertainties, with the exception of the chemical abrasion–isotope dilution–thermal ionization mass spectrometry (CA-ID-TIMS) data from the nonmarine sedimentary basins, which have uncertainties smaller than the symbols. Geochronology is from Metchosin complex (Massey, 1986), Bremerton complex (Haeussler and Clark, 2000), Blue Mountain unit at base of the ~16-km-thick Crescent Formation (Wells et al., 2014), upper Crescent Formation (Babcock et al., 2006), Clayoquot intrusions and Flores volcanics (Irving and Brandon, 1990; Madsen et al., 2006), Walker Creek intrusions (Groome et al., 2003), Mount Pilchuck stock (Yeats and Engels, 1971), and adakite dikes from western Washington (WA; Tepper et al., 2004). All other dates are reported in this paper, with the exception of the date denoted with an asterisk, which was previously reported by Breedlovestrout et al. (2013). MDA—maximum depositional age.

Evans, 1994; Evans and Ristow, 1994; Cheney and Hayman, 2009). However, they have never been presented collectively, nor have geochronologic data been able to confirm their temporal relationships.

We define the lower Swauk basin as those rocks that record W- or SW-directed paleoflow between ≤59.9 and 51.3 Ma in the Chuckanut, Manastash, and Swauk Formations. Sediment accumulation rates for this part of the basin are difficult to determine because of poor exposure and sparse isotopic dates, but rates of ~0.63 m/k.y. for the Chuckanut Formation (Fig. 2) and ~0.60 m/k.y. for the lower Swauk Formation (Fig. 5) are in good agreement and suggest moderately high sediment accumulation during this period. The tectonic setting of the lower Swauk basin remains uncertain. Geophysical data suggest that the boundary between Siletzia and North America represents a Paleogene subduction zone (e.g., Clowes et al., 1987; Hyndman et al., 1990; Gao et al., 2011; Schmandt and Humphreys, 2011), and since the Swauk basin is immediately adjacent to this boundary (Fig. 7), it may represent a forearc basin (Fig. 9A). However, this interpretation is complicated by the absence of arc magmatism in central and western Washington from ca. 60 to 51 Ma (e.g., Miller et al., 2009). This apparent contradiction could be explained by low-angle or flat slab subduction (e.g., Humphreys, 2009), which may also explain the prolonged presence of thick (>30 km), partially molten crust in Washington and British Columbia during much of the Paleocene and early Eocene (Gordon et al., 2008, 2010; Krukenburg et al., 2008). Nevertheless, forearc basins are typically inverted during flat slab subduction (e.g., Finzel et al., 2011), and the steady subsidence of the lower Swauk basin would be anomalous for this setting.

Accretion of Siletzia and Bimodal Volcanism

The upper Swauk basin records a major change in tectonic setting marked by a reversal of paleoflow direction from SSW to NE (Fig. 7), a dramatic increase in sediment accumulation rate to >1.61 m/k.y. (Fig. 5), and, in places, abundant conglomerate clasts likely sourced from rocks in the western and eastern mélange belts (Fig. 1B) between 51.3 and 49.9 Ma (Fig. 8). We infer this change to mark the development of near-trench topography during accretion of Siletzia, and we propose that the upper Swauk basin acted as a foreland basin during this collision (Fig. 9B). Regionally extensive, W-verging fold-and-thrust belts of Eocene age are associated with the accretion of Siletzia on Vancouver Island (Johnston and Acton, 2003) and in Oregon (Wells et al., 2014), but one has

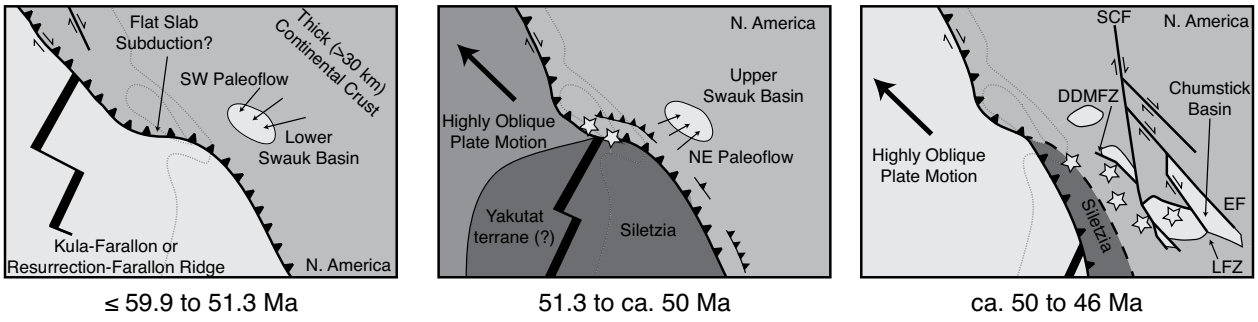

Figure 9. Cartoon maps showing our proposed tectonic evolution of Washington and surrounding area (dashed line denotes modern coastline) ca. 60–45 Ma as described in the text. Abbreviations: DDMFZ—Darrington–Devil's Mountain fault zone, EF—Entiat fault, LFZ—Leavenworth fault zone, and SCF—Straight Creek–Fraser fault. Stars denote the location of Paleogene adakites, peraluminous granites, bimodal volcanism, and other near-trench magmatism. The basaltic Yakutat terrane is shown emplaced adjacent to Siletzia (e.g., Wells et al., 2014), prior to its northward transport and modern collision with southern Alaska.

not been described from western Washington. Nevertheless, the lack of a well-described Eocene fold-and-thrust belt in this area need not preclude its existence, because bedrock of Eocene-age or older is largely covered by rocks related to the modern Cascade arc or Quaternary deposits to the SW of the Swauk basin (Fig. 1B). Interestingly, the exhumed midcrustal rocks of the Skagit gneiss complex (Fig. 1B) also record NE-SW–directed shortening between ca. 51 and >46 Ma (Wintzer, 2012), suggesting that the accretion of Siletzia may have led to shortening in both the upper and middle crust.

Most bathymetric features on the ocean floor subduct easily, leaving little or no geologic record. Two exceptions are thick (>30 km) or young (<10 m.y.) oceanic lithosphere, which is buoyant enough to resist subduction and cause uplift and deformation in the upper plate of a subduction zone (e.g., Cloos, 1993). Siletzia may have represented lithosphere with both of these features. The exposed portion of northern Siletzia is much thicker (10–20 km) than typical oceanic crust (Wells et al., 2014), and existing geochronology suggests that northern Siletzia was formed after 52 Ma (Fig. 8). Interestingly, detrital zircons from the base of the Crescent Formation, which forms the thickest part (~16 km) of northern Siletzia, overlap in age with ca. 51.5–50.5 Ma $^{40}Ar/^{39}Ar$ dates from the top of the formation (Fig. 8) and imply that this sequence was erupted immediately prior to, or concurrent with, accretion. Nevertheless, Wells et al. (2014) reported a date of 46 Ma for one detrital zircon from the base of the Crescent Formation, and if this analysis is accurate, it would require a complex magmatic history for this part of Siletzia that includes voluminous pre-, syn-, and post-accretion magmatism.

Following accretion of Siletzia, thick sequences of basalt with minor rhyolite were emplaced throughout much of the former Swauk basin and are preserved as the Teanaway Formation, Basalt of Frost Mountain, Naches Formation, and Barlow Pass volcanics. The initiation of this volcanic episode is dated in three locations and occurred between 49.933 ± 0.059 Ma and 49.341 ± 0.033 Ma, but its termination is poorly constrained (Fig. 8).

Strike-Slip Faulting

As described already, abundant evidence exists for syndepositional strike-slip faulting on the Entiat and Eagle Creek faults during deposition of the ≤46.902 ± 0.076 Ma to >44.447 ± 0.027 Ma Nahahum Canyon Member of the Chumstick Formation and on the Leavenworth fault zone during deposition of the ca. 49–47 Ma Tumwater Mountain Member of the Chumstick Formation. It is unclear whether the Entiat fault was active prior to ca. 47 Ma. However, the ca. 49–47 Ma Clark Canyon Member of the Chumstick Formation records westerly paleoflow, high sediment accumulation rates (2–7 m/k.y.), and rapid lateral movement of depocenters (Evans, 1994; Johnson, 1996). These features are consistent with deposition in a strike-slip basin, and we suggest that both the Entiat and Leavenworth fault zones were active during deposition of the Clark Canyon Member

Two other high-angle fault systems in western Washington record dextral displacements during the early to middle Eocene. The Straight Creek–Fraser fault displaces the Swauk basin and pre-Cenozoic rocks 100–150 km, requiring this displacement to have occurred after ca. 50 Ma and before the structure was sealed by 35–30 Ma granite intrusions (Tabor et al., 2003). To the north of our field area, the Straight Creek–Fraser fault cuts the Yalakom fault and offsets it ~100 km from its likely southern continuation as the Ross Lake fault. Deformed granites along the Yalakom fault are as young as 48–46 Ma, indicating that ~100 km of dextral displacement occurred on the Straight Creek–Fraser fault after 46 Ma in this area (Coleman and Parrish, 1991). Motion on the Darrington–Devil's Mountain fault zone (Fig. 1B) is also constrained to after ca. 50 Ma, because this structure cuts the SE Chuckanut Formation and displaces blocks of the Manastash Formation along dextral faults (Tabor, 1994).

Return to Regional Depositional System

The Deadhorse Canyon Member of the Chumstick Formation shows no evidence for syndepositional faulting, has paleocurrent indicators that suggest W to SW paleoflow, and is deposited on both sides of the Entiat and Eagle Creek fault zones (Evans, 1994). Therefore, major motion on these structures ceased prior to its deposition. We follow Evans (1994) and correlate these rocks with the Roslyn Formation, which also records W-directed paleoflow, lacks tuffs, and lacks evidence for syndepositional faulting (Walker, 1980; Tabor et al., 1984; Barnett, 1985). Collectively, we refer to the Deadhorse Canyon Member of the Chumstick Formation and the Roslyn Formation as the Roslyn basin (Table 2) and consider it to represent the return of a regional depositional system along this part of the North American margin ≤45.910 ± 0.021 Ma, with a possible western continuation in the Puget Group (Fig. 1B; Vine, 1969, Buckovic, 1979). However, the connection between these two areas remains

uncertain, because the Straight Creek–Fraser fault may have been active during this time (e.g., Coleman and Parrish, 1990; Umhoefer and Miller, 1996).

RELATIONSHIP TO TRIPLE JUNCTION MIGRATION

Plate reconstructions require the subduction of the Kula-Farallon or both the Kula-Resurrection and Resurrection-Farallon Ridges along the North American margin during the Paleogene (e.g., Atwater, 1970; Wells et al., 1984; Engebretson et al., 1985; Haeussler et al., 2003; Madsen et al., 2006). Eocene near-trench magmatism (Cowan, 2003; Groome et al., 2003; Haeussler et al., 2003; Madsen et al., 2006) and geochemically anomalous backarc magmatism (Breitsprecher et al., 2003; Ickert et al., 2009) in southern British Columbia and Washington have been linked to this tectonic setting. The sedimentary, volcanic, and structural history of the Swauk, Chumstick, and Roslyn basins is also consistent with triple junction migration, and we discuss their evolution within this framework.

Near-trench magmatism is typically associated with areas of ridge-trench interaction (e.g., Marshak and Karig, 1977) and can result from a variety of processes. In areas where triple junction geometry results in the formation of a slab window, near-trench magmatism can arise from decompression melting as asthenospheric mantle rises through slab gaps and crustal melting as metasedimentary rocks in the forearc are heated (DeLong et al., 1979; Groome and Thorkelson, 2009). Geochemically anomalous magmas are expected in this setting and include crustal melts (e.g., Hill et al., 1981; Barker et al., 1992) and adakites (Thorkelson and Breitsprecher, 2005). Alternatively, the formation and capture of oceanic microplates can also occur during ridge-trench interaction (e.g., Stock and Lee, 1994) and is sometimes associated with slab breakoff, which can lead to similar magmatism (Ferrari, 2004; Pallares et al., 2007).

Early Eocene near-trench magmatism on southern Vancouver Island and in western Washington includes peraluminous granites that represent melts derived from forearc metasedimentary rocks and dacitic rocks with adakitic geochemistry that may represent melts derived from subducted basalt or underplated mafic crust. Dated near-trench magmatism includes the ca. 51 Ma, peraluminous Walker Creek intrusions (Fig. 1B; Groome et al., 2003), the ca. 49 Ma, peraluminous Mount Pilchuck intrusive suite (Fig. 1B; Wiebe, 1963; Yeats and Engels, 1971), ca. 48–47 Ma dacitic dikes with adakitic compositions that intrude northern Siletzia in the Bremerton Hills (Fig. 1B; Tepper et al., 2004), and the ca. 51–49 Ma Flores volcanics and Clayoquot intrusions on Vancouver Island (Irving and Brandon, 1990; Madsen et al., 2006). Undated adakite localities include block-and-ash-flow deposits near Port Townsend (Fig. 1B; Tepper et al., 2004) and dacite in the ca. 47–36 Ma Mount Persis volcanics (Fig. 1B; Macdonald et al., 2013). All of this near-trench magmatism occurred over a short interval between ca. 51 and 47 Ma (Fig. 8) and has similar compositional diversity to near-trench magmatic suites in areas where ridge-trench interaction is well documented, including the southern Alaska margin (Hill et al., 1981; Barker et al., 1992; Harris et al., 1996) and Taitao Peninsula in Chile (Forsythe et al., 1986; Kaeding et al., 1990; Guivel et al., 1999). These similarities have led Cowan (2003), Groome et al. (2003), Haeussler et al. (2003), and Madsen et al. (2006) to suggest that the near-trench magmatism in western Washington and on Vancouver Island occurred at a ridge-trench-trench triple junction, and we follow these authors by placing either the Kula–Farallon–North America or Resurrection–Farallon–North America triple junction on Vancouver Island between 51 and 49 Ma (Fig. 9B). Dates for near-trench magmatism in Washington are slightly younger than those on Vancouver Island (Fig. 8), albeit still within uncertainty, and may indicate that the triple junction was migrating southward at this time.

Initial disruption of the Swauk basin coincided with the earliest forearc magmatism on Vancouver Island at ca. 51 Ma (Figs. 8 and 9) and was likely caused by accretion of both young (<2 Ma) and thick (10–20 km) oceanic crust belonging to Siletzia. The tectonic setting required to generate such thickened crust remains enigmatic. However, the projected position of the Yellowstone hotspot during the Paleogene is in western Oregon (Johnston and Thorkelson, 2000), and northern Siletzia may represent oceanic crust developed at a spreading ridge influenced by the presence of a mantle plume (e.g., McCrory and Wilson, 2013; Wells et al., 2014). The attempted subduction of northern Siletzia culminated in the development of a WNW-trending fold-and-thrust belt in the Swauk basin between 51.3 and 49.9 Ma (Fig. 9B) and was followed by bimodal volcanism.

Uplift and the development of unconformities have been documented in other forearc basins during ridge-trench interaction (e.g., Gulick et al., 2002; Trop et al., 2003), indicating that it might be a common effect of this process. The driving force behind uplift may be shortening related to the subduction of young, buoyant crust (e.g., Cloos, 1993), development of dynamic topography above slab windows (e.g., Groome and Thorkelson, 2009; Guillaume et al., 2010), or some combination of the two processes. In the Swauk basin, shortening is linked to the accretion of Siletzia, which likely represented young, thick, and buoyant oceanic crust. The attempted subduction of such anomalous crust may explain why shortening occurred from Vancouver Island to southern Oregon (Johnston and Acton, 2003; Wells et al., 2014), compared to the less pronounced shortening described from the Matanuska Valley–Talkeetna Mountains basin during Paleogene ridge-trench interaction (Trop et al., 2003) or the more localized uplift and shortening associated with the modern Mendocino triple junction (McCrory, 2000; Gulick et al., 2002).

Dextral strike-slip faulting began, or accelerated, on the Entiat, Leavenworth, Darrington–Devil's Mountain, Eagle Creek, and Straight Creek–Fraser fault zones in western Washington immediately following the accretion of Siletzia at 51.3–49.9 Ma and lasted 5–15 m.y. Precise estimates for the offset on most of these faults are not available. However, we interpret the 100–150 km of post–ca. 50 Ma displacement on the Straight Creek-Fraser fault as well as the initiation, or acceleration, of dextral motion on the other fault systems described in this paper to be indicative of a change to significant dextral motion along this part of the North American plate boundary. These faults form the southern portion of series of major strike-slip faults that run through the northern Cordillera, each of which records large dextral displacements (>100 km) during the Late Cretaceous and early Cenozoic (Lanphere, 1978; Gabrielse, 1985; Wyld et al., 2006; Pavlis and Roeske, 2007). The driving force for this faulting was oblique motion between the Kula, and possibly the Resurrection, plate(s) and North America, and we infer that the initiation, or acceleration, of strike-slip motion in central and western Washington marks the southward migration, or jump, of the Kula–Farallon–North America or Resurrection–Farallon–North America triple junction following accretion of Siletzia (Fig. 9C).

Near-trench magmatism to the south of our field area that may mark the location of the triple junction after the events discussed in this paper includes a regional series of gabbroic sills that are found from western Washington to southern Oregon constrained to between 46 and 42 Ma in age and the 42–34 Ma bimodal Tillamook, Yachats, Cascade Head, and Grays River volcanics (Chan et al., 2012; Wells et al., 2014). However, the tectonic setting for this magmatism is controversial, and it may represent near-trench magmatism related to ridge-trench interaction (Wells et al., 1984; Madsen et al., 2006),

magmatism related to the Yellowstone hotspot (Wells et al., 2014), or a combination of the two settings (Chan et al., 2012).

CONCLUSIONS

The relationship between structurally isolated Paleogene nonmarine sedimentary sequences in central and western Washington has been a long-standing problem. The high-precision U-Pb zircon geochronology presented in this paper allows their temporal correlation and reveals a semicontinuous and self-consistent stratigraphy from ca. 60 to 45 Ma. Restoration of 100–150 km of dextral motion on the Straight Creek–Fraser fault places the Chuckanut, Manastash, and Swauk Formations adjacent to one another, and, on the basis of sedimentological and temporal similarities, we consider these formations to have formed a single sedimentary basin from ≤59.9 to >49.9 Ma, which we call the Swauk basin. This basin was deposited along westward-flowing streams from ≤59.9 Ma to 51.3 Ma, but it experienced significant disruption between 51.3 Ma and >49.9 Ma, starting with a reversal in paleoflow direction and culminating in basin inversion and the development of a WNW-trending fold belt that we attribute to the attempted subduction of young, thick, and buoyant oceanic crust belonging to Siletzia. Following the accretion of Siletzia, the Swauk basin was dismembered by dextral strike-slip faults, and the Chumstick strike-slip basin formed between the Entiat and Leavenworth faults. Sedimentary rocks belonging to the Roslyn basin are ≤45.9 Ma and span the Entiat, Eagle Creek, and Leavenworth fault zones, precluding significant strike-slip faulting on these structures during its deposition. However, strike-slip faulting may have continued on the Straight Creek–Fraser fault until 35–30 Ma. The record of Paleogene sediment accumulation, volcanism, and strike-slip faulting described in this paper can be linked to events along the plate margin, and we consider the initiation, or acceleration, of dextral strike-slip faulting in central and western Washington to mark the southward migration of the Kula-Farallon or Resurrection-Farallon Ridge along the North American margin. This interpretation is consistent with the timing of near-trench and geochemically anomalous backarc magmatism at this latitude, and it provides further support for the presence of one of these ridges along this part of the Pacific Northwest during the early Eocene.

APPENDIX A

Zircons were separated from each sample using standard crushing and density separation techniques. Rocks were first sledged to <1 cm^3 pieces and then subjected to repeated short-duration runs (<5 s) in a Spex Shatterbox in an effort to liberate individual mineral grains. This material was then sieved through a 500 µm mesh, and the resulting <500 µm fraction was washed by hand for an initial, crude density separation. The remaining sample was run through a Frantz magnetic separator at 0.6 A/20°. A final density separation was done using methyl iodide (MeI) on the nonmagnetic fraction, and a pure zircon separate was obtained by handpicking under a binocular microscope.

Individual zircons selected for CA-ID-TIMS analysis were annealed at 900 °C for 60 h and then partially digested in 29 *M* HF in a Parr vessel held at 215 °C for 12 h. The partially digested grains were rinsed in ultrapure H_2O, fluxed on a hot plate (~80 °C) in 6.2 *N* HCl, re-rinsed in ultrapure H_2O, and loaded into individual Teflon microcapsules. The capsules were spiked with the EARTHTIME ^{205}Pb-^{233}U-^{235}U isotopic tracer (Condon et al., 2015), and the partially digested grains were completely dissolved in 29 *M* HF in a Parr vessel held at 215 °C for 48 h. The resulting solutions were dried down, dissolved in 6.2 *N* HCl, and held at 180 °C for ~12 h. Samples were then converted to 3 *N* HCl, and U and Pb were separated on anion exchange columns following the procedure of Krogh (1973). The samples were then dried down to a chloride salt, redissolved in silica gel, and loaded onto outgassed, zone-refined Re filaments for TIMS analysis.

All isotopic measurements were made on either the VG Sector 54 or Isotopx X62 TIMS at the Massachusetts Institute of Technology. Pb isotopes were measured by peak hopping on a Daly detector and corrected for fractionation based on repeat analyses of the NBS 981 Pb isotopic standard. U was measured statically on Faraday cups and corrected for fractionation using the ^{233}U-^{235}U double spike. We assumed that zircon grains incorporated no initial Pb during crystallization and that all measured ^{204}Pb came from the laboratory blank (Pb_c). The mass of Pb_c measured in all the analyses in this paper is indistinguishable from the range of Pb_c seen in total procedural blanks and provides strong support for the assumption. We corrected all Pb isotopic ratios for laboratory blank using $^{206}Pb/^{204}Pb = 17.910828 \pm 0.371937$, $^{207}Pb/^{204}Pb = 15.204620 \pm 0.261366$, and $^{208}Pb/^{204}Pb = 36.841963 \pm 0.726065$ (1σ, absolute) based on 53 total procedural blanks measured between August 2013 and January 2015. All analyses were corrected for exclusion of ^{230}Th during zircon crystallization. The ^{230}Th isotope is a long-lived (half-life [$t^{1/2}$] = 75.380 k.y.) daughter product of ^{238}U, and its preferential exclusion from zircon can result in a $^{238}U/^{206}Pb$ date that is too young by as much as ~100 k.y. We corrected for this initial ^{230}Th deficiency using a calculated Th/U for the zircon and an assumed Th/U ratio of 2.8 ± 1 (2σ) for the magma (Machlus et al., 2015). Data reduction was done using the U-Pb_Redux software package (Bowring et al., 2011) and used the decay constants for ^{238}U and ^{235}U presented in Jaffey et al. (1971). All isotopic data are reported in Table DR1 and shown on concordia plots in Figure DR1 (see footnote 1). Only the youngest population of zircon dates for each sample is shown in Figure DR1 (see footnote 1). For dates of zircon grains that we interpret as detrital, please refer to Table DR1 (see footnote 1).

Dates for four of the samples presented in this paper were previously reported in McLean (2011) and differ by up to ~20 k.y. This difference arises from additional zircon analyses and the application of a new laboratory blank isotopic composition.

ACKNOWLEDGMENTS

We thank Jim Evans and Joe Vance for sharing the location of tuffs within the studied sedimentary sequences, and E. Barry, T. LaCasse, E. Shorin, Y. Park, and J. Pu for field and laboratory assistance. Funding for this project was provided by National Science Foundation grants EAR-0510591 and EAR-1118883 to Bowring, EAR-0511062 and EAR-1119358 to Miller, and EAR-1119063 to Umhoefer. This manuscript benefited from reviews by S.T. Johnston, D.J. Thorkelson, and R.E. Wells.

REFERENCES CITED

Atwater, T., 1970, Implications of plate tectonics for the Cenozoic tectonic evolution of North America: Geological Society of America Bulletin, v. 81, p. 3513–3536, doi:10.1130/0016-7606(1970)81[3513:IOPTFT]2.0.CO;2.

Babcock, R.S., Hirsch, D.M., and Clark, K.P., 2006, Geochemistry and petrology of a thick sequence of Crescent basalt in the Dosewallips River Valley, Olympic Peninsula, Washington State: Geological Society of America Abstracts with Programs, v. 38, no. 5, p. 95.

Barker, F., Farmer, G.L., Ayuso, R.A., Plafker, G., and Lull, J.S., 1992, The 50 Ma granodiorite of the eastern Gulf of Alaska: Melting in an accretionary prism in the forearc: Journal of Geophysical Research–Solid Earth, v. 97, p. 6757–6778, doi:10.1029/92JB00257.

Barnett, D.B., 1985, A Paleoenvironmental Reconstruction of the Upper Roslyn Formation, Central Washington, with Implications for Coal Exploration [M.S. thesis]: Cheney, Washington, Eastern Washington University, 334 p.

Benoit, M., Aguillon-Robles, A., Calmus, T., Maury, R.C., Bellon, H., Cotton, J., Bourgois, J., and Michaud, F., 2002, Geochemical diversity of late Miocene volcanism in southern Baja California, Mexico: Implication of mantle and crustal sources during the opening of an asthenospheric window: The Journal of Geology, v. 110, p. 627–648, doi:10.1086/342735.

Bowring, J.F., McLean, N.M., and Bowring, S.A., 2011, Engineering cyber infrastructure for U-Pb geochronology: Tripoli and U-Pb_Redux: Geochemistry Geophysics Geosystems, v. 12, p. Q0AA19, doi:10.1029/2010GC003479.

Bradley, D.C., Kusky, T., Haeussler, P.J., Goldfarb, R., Miller, M.L., Dumoulin, J., Nelson, S.W., and Karl, S., 2003, Geologic signature of Early Tertiary ridge subduction in Alaska, *in* Sisson, V.B., Roeske, S.M., and Pavlis, T.L., eds., Geology of a Transpressional Orogen Developed During Ridge-Trench Interaction Along the North Pacific Margin: Geological Society of America Special Paper 371, p. 19–49, doi:10.1130/0-8137-2371-X.19.

Breedlovestrout, R.L., 2011, Paleofloristic Studies in the Paleogene Chuckanut Basin, Western Washington, USA [Ph.D. thesis]: Moscow, Idaho, University of Idaho, 954 p.

Breedlovestrout, R.L., Evraets, B.J., and Parrish, J.T., 2013, New Paleogene paleoclimate analysis of western Washington using physiognomic characteristics from fossil leaves: Palaeogeography, Palaeoclimatology, Palaeoecology, v. 392, p. 22–40, doi:10.1016/j.palaeo.2013.08.013.

Breitsprecher, K., Thorkelson, D.J., Groome, W.G., and Dostal, J., 2003, Geochemical confirmation of the Kula-Farallon slab window beneath the Pacific Northwest in Eocene time: Geology, v. 31, p. 351–354, doi:10.1130/0091-7613(2003)031<0351:GCOTKF>2.0.CO;2.

Buckovic, W.A., 1979, The Eocene deltaic system of west-central Washington, *in* Armentrout, J.M., Cole, M.R., and TerBest, H., eds., Cenozoic Paleogeography of the Western United States: Los Angeles, California, Society of Economic Paleontologists and Mineralogists, Pacific Coast Section, Pacific Coast Paleogeography Symposium 3, p. 147–164.

Chan, C.F., Tepper, J.H., and Nelson, B.K., 2012, Petrology of the Grays River volcanics, southwestern Washing-

ton: Plume-influenced slab window magmatism in the Cascadia forearc: Geological Society of America Bulletin, v. 124, p. 1324–1338, doi:10.1130/B30576.1.

Cheney, E.S., 1994, Cenozoic Unconformity-Bounded Sequences of Central and Eastern Washington: Washington Division of Geology and Earth Resources Bulletin 80, p. 115–139.

Cheney, E.S., 2003, Regional Tertiary sequence stratigraphy and regional structure on the eastern flank of the central Cascade Range, Washington, *in* Swanson, T.W., ed., Western Cordillera and Adjacent Areas: Geological Society of America Field Guide 4, p. 177–199, doi:10.1130/0-8137-0004-3.177.

Cheney, E.S., and Hayman, N.W., 2009, The Chiwaukum structural low: Cenozoic shortening of the central Cascade Range, Washington State, USA: Geological Society of America Bulletin, v. 121, p. 1135–1153, doi:10.1130/B26446.1.

Clayton, D.N., 1973, Volcanic History of the Teanaway Basalt, East-Central Cascade Mountains, Washington [M.S. thesis]: Seattle, Washington, University of Washington, 55 p.

Cloos, M., 1993, Lithospheric buoyancy and collisional orogenesis: Subduction of orogenic plateaus, continental margins, island arcs, spreading ridges, and seamounts: Geological Society of America Bulletin, v. 105, p. 715–737, doi:10.1130/0016-7606(1993)105<0715:LBACOS>2.3.CO;2.

Clowes, R.M., Brandon, M.T., Green, A.G., Yorath, C.J., Sutherland Brown, A., Kanasewich, E.R., and Spencer, C., 1987, LITHOPROBE—southern Vancouver Island: Cenozoic subduction complex imaged by deep seismic reflections: Canadian Journal of Earth Sciences, v. 24, p. 31–51, doi:10.1139/e87-004.

Coleman, M.E., and Parrish, R.R., 1991, Eocene dextral strike-slip and extensional faulting in the Bridge River terrane, southwest British Columbia: Tectonics, v. 10, p. 1222–1238, doi:10.1029/91TC01078.

Condon, D.J., Schoene, B., McLean, N.M., Bowring, S.A., and Parrish, R.R., 2015, Metrology and traceability of U-Pb isotope dilution geochronology (EARTHTIME tracer calibration Part I): Geochimica et Cosmochimica Acta, v. 164, p. 464–480, doi:10.1016/j.gca.2015.05.026.

Cowan, D.S., 2003, Revisiting the Baranof–Leech River hypothesis for Early Tertiary coastwise transport of the Chugach–Prince William terrane: Earth and Planetary Science Letters, v. 213, p. 463–475, doi:10.1016/S0012-821X(03)00300-5.

Cruver, S.K., 1981, The Geology and Mineralogy of Bentonites and Associated Rocks of the Chuckanut Formation, Mt. Higgins Area, North Cascades Washington [M.S. thesis]: Bellingham, Washington, Western Washington University, 105 p.

DeLong, S.E., Schwarz, W.M., and Anderson, R.N., 1979, Thermal effects of ridge subduction: Earth and Planetary Science Letters, v. 44, p. 239–246, doi:10.1016/0012-821X(79)90172-9.

Doran, B.A., 2009, Structure of the Swauk Formation and Teanaway Dike Swarm, Washington Cascades [M.S. thesis]: San Jose, California, San Jose State University, 97 p.

Dragovich, J.D., Logan, R.L., Schasse, H.W., Walsh, T.J., Lingley, W.S., Jr., Norman, D.K., Gerstel, W.J., Lapen, T.J., Schuster, E., and Meyers, K.D., 2002, Geologic Map of Washington—Northwest Quadrant: Washington Department of Natural Resources Geologic Map GM-50, scale 1:250,000, 3 sheets, 72 p. text.

Dragovich, J.D., Stanton, B.W., Lingley, W.S., Jr., Griesel, G.A., and Polenz, M., 2003, Geologic Map of the Mount Higgins 7.5-Minute Quadrangle, Skagit and Snohomish Counties, Washington: Washington Division of Geology and Earth Resources Open-File Report 2003-12, scale 1:24,000, 1 sheet.

Einarsen, J.M., 1987, The Petrography and Tectonic Significance of the Blue Mountain Unit, Olympic Peninsula, Washington [M.S. thesis]: Bellingham, Washington, Western Washington University, 175 p.

Engebretson, D.C., Cox, A., and Gordon, R.G., 1985, Relative Motions Between Oceanic and Continental Plates in the Pacific Basin: Geological Society of America Special Paper 206, 60 p., doi:10.1130/SPE206-p1.

Evans, J.E., 1994, Depositional history of the Eocene Chumstick Formation: Implications of tectonic partitioning for the history for the Leavenworth and Entiat–Eagle Creek fault systems, Washington: Tectonics, v. 13, p. 1425–1444, doi:10.1029/94TC01321.

Evans, J.E., 1996, Depositional history of the Eocene Chumstick Formation: Implications of tectonic partitioning for the history for the Leavenworth and Entiat–Eagle Creek fault systems, Washington [Reply]: Tectonics, v. 15, p. 510–514, doi:10.1029/95TC03695.

Evans, J.E., and Ristow, R.J., Jr., 1994, Depositional history of the southeastern outcrop belt of the Chuckanut Formation: Implications for the Darrington–Devil's Mountain and Straight Creek fault zones, Washington (USA): Canadian Journal of Earth Sciences, v. 31, p. 1727–1743, doi:10.1139/e94-154.

Ferrari, L., 2004, Slab detachment control on mafic volcanic pulse and mantle heterogeneity in central Mexico: Geology, v. 32, p. 77–80, doi:10.1130/G19887.1.

Finzel, E.S., Trop, J.M., Ridgeway, K.D., and Enkelmann, E., 2011, Upper plate proxies for flat-slab subduction processes in southern Alaska: Earth and Planetary Science Letters, v. 303, p. 348–360, doi:10.1016/j.epsl.2011.01.014.

Forsythe, R.D., Nelson, E.P., Carr, M.J., Kaeding, M.E., Herve, M., Mpodozis, C., Soffia, J.M., and Harambour, S., 1986, Pliocene near-trench magmatism in southern Chile: A possible manifestation of ridge collision: Geology, v. 14, p. 23–27, doi:10.1130/0091-7613(1986)14<23:PNMISC>2.0.CO;2.

Foster, R.J., 1960, Tertiary geology of a portion of the central Cascade Mountains, Washington: Geological Society of America Bulletin, v. 71, p. 99–126, doi:10.1130/0016-7606(1960)71[99:TGOAPO]2.0.CO;2.

Frizzell, V.A., Jr., 1979, Petrology and Stratigraphy of Paleogene Nonmarine Sandstones, Cascade Range, Washington: U.S. Geological Survey Open-File Report 79-1149, 151 p.

Gabrielse, H., 1985, Major dextral transcurrent displacements along the Northern Rocky Mountain Trench and related lineaments in north-central British Columbia: Geological Society of America Bulletin, v. 96, p. 1–14, doi:10.1130/0016-7606(1985)96<1:MDTDAT>2.0.CO;2.

Gao, H., Humphreys, E.D., Yao, H., and van der Hilst, R.D., 2011, Crust and lithosphere structure of northwestern U.S. with ambient noise tomography: Terrane accretion and Cascade arc development: Earth and Planetary Science Letters, v. 304, p. 202–211, doi:10.1016/j.epsl.2011.01.033.

Gilmour, L.A., 2012, U/Pb ages of Eocene and Younger Rocks on the Eastern Flank of the Central Cascade Range, Washington, USA [M.S. thesis]: Seattle, Washington, University of Washington, 48 p.

Gordon, S.M., Whitney, D.L., Teyssier, C., Grove, M., and Dunlap, W.J., 2008, Timescales of migmatization, melt crystallization, and cooling in a Cordilleran gneiss dome: Valhalla complex, southeastern British Columbia: Tectonics, v. 27, TC4010, doi:10.1029/2007TC002103.

Gordon, S.M., Bowring, S.A., Whitney, D.L., Miller, R.B., and McLean, N.M., 2010, Timescales of metamorphism, deformation, and crustal melting in a continental arc, North Cascades, USA: Geological Society of America Bulletin, v. 122, p. 1308–1330, doi:10.1130/B30060.1.

Gresens, R.L., Naeser, C.W., and Whetten, J.W., 1981, Stratigraphy and age of the Chumstick and Wenatchee Formations: Tertiary fluvial and lacustrine rocks, Chiwaukum graben, Washington: Geological Society of America Bulletin, v. 92, p. 841–876, doi:10.1130/GSAB-P2-92-841.

Groome, W.G., and Thorkelson, D.J., 2009, The three-dimensional thermo-mechanical signature of ridge subduction and slab window migration: Tectonophysics, v. 464, p. 70–83, doi:10.1016/j.tecto.2008.07.003.

Groome, W.G., Thorkelson, D.J., Friedman, R.M., Mortensen, J.K., Massey, N.W.D., Marshall, D.D., and Layer, P.W., 2003, Magmatic and tectonic history of the Leech River complex, Vancouver Island, British Columbia: Evidence for ridge-trench intersection and accretion of the Crescent terrane, *in* Sisson, V.B., Roeske, S.M., and Pavlis, T.L., eds., Geology of a Transpressional Orogen Developed During Ridge-Trench Interaction Along the North Pacific Margin: Geological Society of America Special Paper 371, p. 327–353, doi:10.1130/0-8137-2371-X.327.

Grow, J.A., and Atwater, T., 1970, Mid-Tertiary tectonic transition in the Aleutian arc: Geological Society of America Bulletin, v. 81, p. 3715–3722, doi:10.1130/0016-7606(1970)81[3715:MTTITA]2.0.CO;2.

Guillaume, B., Moroni, M., Funiciello, F., Martinod, J., and Faccenna, C., 2010, Mantle flow and dynamic topography associated with slab window opening: Insights from laboratory models: Tectonophysics, v. 496, p. 83–98, doi:10.1016/j.tecto.2010.10.014.

Guivel, C., Lagabrielle, Y., Bourgois, J., Maury, R.C., Fourcade, S., Martin, H., and Arnaud, N., 1999, New geochemical constraints for the origin of ridge-subduction–related plutonic and volcanic suites from the Chile triple junction (Taitao Peninsula and Site 862, ODP Leg 141 on the Taitao Ridge): Tectonophysics, v. 311, p. 83–111, doi:10.1016/S0040-1951(99)00160-2.

Gulick, S.P.S., Meltzer, A.S., and Clarke, S.H., Jr., 2002, Effect of the northward-migrating Mendocino triple junction on the Eel River forearc basin, California: Stratigraphic development: Geological Society of America Bulletin, v. 114, p. 178–191, doi:10.1130/0016-7606(2002)114<0178:EOTNMM>2.0.CO;2.

Haeussler, P.J., and Clark, K.P., 2000, Geologic Map of the Wildcat Lake 7.5′ Quadrangle, Kitsap and Mason Counties, Washington: U.S. Geological Survey Open-File Report 2000-356, scale 1:24,000.

Haeussler, P.J., Bradley, D.C., Wells, R.E., and Miller, M.L., 2003, Life and death of the Resurrection plate: Evidence for its existence and subduction in the northeastern Pacific in Paleocene–Eocene time: Geological Society of America Bulletin, v. 115, p. 867–880, doi:10.1130/0016-7606(2003)115<0867:LADOTR>2.0.CO;2.

Harris, N.R., Sisson, V.B., Wright, J.E., and Pavlis, T.L., 1996, Evidence for Eocene mafic underplating during forearc intrusive activity, eastern Chugach Mountains, Alaska: Geology, v. 24, p. 263–266, doi:10.1130/0091-7613(1996)024<0263:EFEMUD>2.3.CO;2.

Hill, M., Morris, J., and Whelan, J., 1981, Hybrid granodiorites intruding the accretionary prism, Kodiak, Shumagin, and Sanak islands, southwest Alaska: Journal of Geophysical Research–Solid Earth, v. 86, p. 10,569–10,590, doi:10.1029/JB086iB11p10569.

Humphreys, E., 2009, Relation of flat subduction to magmatism and deformation in the western United States, *in* Kay, S.M., Ramos, V.A., and Dickinson, W.R., eds., Backbone of the Americas: Shallow Subduction, Plateau Uplift, and Ridge and Terrane Collision: Geological Society of America Memoir 204, p. 85–98, doi:10.1130/2009.1204(04).

Hyndman, R.D., Yorath, C.J., Clowes, R.M., and Davis, E.E., 1990, The northern Cascadia subduction zone at Vancouver Island: Seismic structure and tectonic history: Canadian Journal of Earth Sciences, v. 27, p. 313–329, doi:10.1139/e90-030.

Ickert, R.B., Thorkelson, D.J., Marshall, D.D., and Ullrich, T.D., 2009, Eocene adakitic volcanism in southern British Columbia: Remelting of arc basalt above a slab window: Tectonophysics, v. 464, p. 164–185, doi:10.1016/j.tecto.2007.10.007.

Irving, E., and Brandon, M.T., 1990, Paleomagnetism of the Flores volcanics, Vancouver Island, in place by Eocene time: Canadian Journal of Earth Sciences, v. 27, p. 811–817, doi:10.1139/e90-083.

Jaffey, A.H., Flynn, K.F., Glendenin, L.E., Bentley, W.C., and Essling, A.M., 1971, Precision measurement of half-lives and specific activities of ^{235}U and ^{238}U: Physical Review C, Nuclear Physics, v. 4, p. 1889–1906, doi:10.1103/PhysRevC.4.1889.

Johnson, C.M., and O'Neil, J.R., 1984, Triple junction magmatism: A geochemical study of Neogene volcanic rocks in western California: Earth and Planetary Science Letters, v. 71, p. 241–262, doi:10.1016/0012-821X(84)90090-6.

Johnson, S.Y., 1984, Stratigraphy, age, and paleogeography of the Eocene Chuckanut Formation, northwest Wash-

ington: Canadian Journal of Earth Sciences, v. 21, p. 92–106, doi:10.1139/e84-010.

Johnson, S.Y., 1985, Eocene strike-slip faulting and nonmarine basin formation in Washington, *in* Biddle, K.T., and Christie-Blick, N., eds., Strike-Slip Deformation, Basin Formation and Sedimentation: Society of Economic Paleontologists and Mineralogists Special Publication 37, p. 283–302.

Johnson, S.Y., 1996, Depositional history of the Eocene Chumstick Formation: Implications of tectonic partitioning for the history of the Entiat–Eagle Creek fault systems, Washington [Comment]: Tectonics, v. 15, p. 506–509, doi:10.1029/95TC03694.

Johnson, S.Y., and O'Connor, J.T., 1994, Stratigraphy, Sedimentology, and Provenance of the Raging River Formation (Early? and Middle Eocene), King County, Washington: U.S. Geological Survey Bulletin 2085-A, p. A1–A33.

Johnston, S.T., and Acton, S., 2003, The Eocene southern Vancouver Island orocline—Seamount accretion and the cause of fold-and-thrust belt and extensional basin formation: Tectonophysics, v. 365, p. 165–183, doi:10.1016/S0040-1951(03)00021-0.

Johnston, S.T., and Thorkelson, D.J., 2000, Continental flood basalts: Episodic magmatism above long-lived hotspots: Earth and Planetary Science Letters, v. 175, p. 247–256, doi:10.1016/S0012-821X(99)00293-9.

Kaeding, M., Forsythe, R.D., and Nelson, E.P., 1990, Geochemistry of the Taitao ophiolite and near-trench intrusions from the Chile margin triple junction: Journal of South American Earth Sciences, v. 3, p. 161–177, doi:10.1016/0895-9811(90)90001-H.

Krogh, T.E., 1973, Low-contamination method for hydrothermal decomposition of zircon and extraction of U and Pb for isotopic age determinations: Geochimica et Cosmochimica Acta, v. 37, p. 485–494, doi:10.1016/0016-7037(73)90213-5.

Krukenburg, S.C., Whitney, D.L., Teyssier, C., Fanning, C.M., and Dumlap, W.J., 2008, Paleocene–Eocene migmatite crystallization, extension, and exhumation in the hinterland of the northern Cordillera: Okanogan dome, Washington, USA: Geological Society of America Bulletin, v. 120, p. 912–929, doi:10.1130/B26153.1.

Lanphere, M.A., 1978, Displacement history of the Denali fault system, Alaska and Canada: Canadian Journal of Earth Sciences, v. 15, p. 817–822, doi:10.1139/e78-086.

MacDonald, J.H., Dragovich, J.D., Littke, H.A., Anderson, M., and Dufrane, A.S., 2013, The volcanic rocks of Mount Persis: An Eocene continental arc that contains adakitic magmas: Geological Society of America Abstracts with Programs, v. 45, no. 7, p. 392.

Machlus, M.L., Ramezani, J., Bowring, S.A., Hemming, S.R., Tsukui, K., and Clyde, W.C., 2015, A strategy for cross-calibrating U-Pb chronology and astrochronology of sedimentary sequences: An example from the Green River Formation, Wyoming, USA: Earth and Planetary Sciences, v. 413, p. 70–78, doi:10.1016/j.epsl.2014.12.009.

Madsen, J.K., Thorkelson, D.J., Friedman, R.M., and Marshall, D.D., 2006, Cenozoic to recent plate configurations in the Pacific Basin: Ridge subduction and slab window magmatism in western North America: Geosphere, v. 2, p. 11–34, doi:10.1130/GES00020.1.

Marshak, R.S., and Karig, D.E., 1977, Triple junctions as a cause for anomalously near-trench igneous activity between the trench and volcanic arc: Geology, v. 5, p. 233–236, doi:10.1130/0091-7613(1977)5<233:TJAACF>2.0.CO;2.

Massey, N.W., 1986, Metchosin igneous complex, southern Vancouver Island: Ophiolite stratigraphy developed in an emergent island setting: Geology, v. 14, p. 602–605, doi:10.1130/0091-7613(1986)14<602:MICSVI>2.0.CO;2.

Massey, N.W., MacIntyre, D.G., Desjardins, P.J., and Cooney, R.T., 2005, Geology of British Columbia: British Columbia Ministry of Energy, Mines, and Petroleum Resources Geoscience Map 2005-3, scale 1:1,000,000, 3 sheets.

Mattinson, J.M., 2005, Zircon U-Pb chemical abrasion ("CA-TIMS") method: Combined annealing and multi-step partial dissolution analysis for improved precision and accuracy of zircon ages: Chemical Geology, v. 220, p. 47–66, doi:10.1016/j.chemgeo.2005.03.011.

McClincy, M.J., 1986, Tephrostratigraphy of the Middle Eocene Chumstick Formation, Cascade Range, Douglas County, Washington [M.S. thesis]: Portland, Oregon, Portland State University, 254 p.

McCrory, P.A., 2000, Upper plate contraction north of the migrating Mendocino triple junction, northern California: Implications for the partitioning of strain: Tectonics, v. 19, p. 1144–1160, doi:10.1029/1999TC001177.

McCrory, P.A., and Wilson, D.S., 2013, A kinematic model for the formation of the Siletz-Crescent forearc terrane by capture of coherent fragments of the Farallon and Resurrection plates: Tectonics, v. 32, p. 718–736, doi:10.1002/tect.20045.

McLean, N.M., 2011, Statistical Considerations in High Precision U-Pb Geochronology with an Application to the Tectonic Evolution of the North Cascades, Washington [Ph.D. thesis]: Cambridge, Massachusetts, Massachusetts Institute of Technology, 186 p.

Miller, G.M., and Misch, P., 1963, Early Eocene angular unconformity at western front of northern Cascades, Whatcom County, Washington: American Association of Petroleum Geologists Bulletin, v. 47, p. 163–174.

Miller, R.B., Gordon, S.M., Bowring, S.A., Doran, B.A., McLean, N.M., Michels, Z.D., Shea, E.K., Whitney, D.L., Wintzer, N.E., and Mendoza, M.K., 2009, Linking deep and shallow crustal processes in an exhumed continental arc, North Cascades, Washington, *in* O'Connor, J.E., Dorsey, R.J., and Madin, I.P., eds., Volcanoes to Vineyards: Geologic Field Trips Through the Dynamic Landscape of the Pacific Northwest: Geological Society of America Field Guide 15, p. 373–406, doi:10.1130/2009.fld015(19).

Pallares, C., Maury, R.C., Bellon, H., Royer, J., Calmus, T., Aguillon-Robles, A., Cotton, J., Benoit, M., Michaud, F., and Bourgois, J., 2007, Slab-tearing following ridge-trench collisions: Evidence from Miocene volcanism in Baja California, Mexico: Journal of Volcanology and Geothermal Research, v. 161, p. 95–117, doi:10.1016/j.jvolgeores.2006.11.002.

Pavlis, T.L., and Roeske, S.M., 2007, The Border Ranges fault system, southern Alaska, *in* Ridgeway, K.D., Trop, J.M., Glen, J.M., and O'Neill, M.J., eds., Tectonic Growth of a Collisional Continental Margin: Crustal Evolution of Southern Alaska: Geological Society of America Special Paper 431, p. 95–127, doi:10.1130/2007.2431(05).

Schmandt, B., and Humphreys, E., 2011, Seismically imaged relict slab from the 55 Ma Siletzia accretion to the northwest United States: Geology, v. 39, p. 175–178, doi:10.1130/G31558.1.

Schuster, J.E., Gulick, C.W., Reidel, S.P., Fecht, K.R., and Zurenko, S., 1997, Geologic Map of Washington—Northeast Quadrant: Washington Division of Geology and Earth Resources Geologic Map GM-45, scale 1:250,000, 2 sheets, 20 p. text.

Stock, J.M., and Lee, J., 1994, Do microplates in subduction zones leave a geological record?: Tectonics, v. 13, p. 1472–1487, doi:10.1029/94TC01808.

Stoffel, K.L., Joseph, N.L., Waggoner, S.Z., Gulick, C.W., Korosec, M.A., and Bunning, B.B., 1991, Geologic Map of Washington—Northeast Quadrant: Washington Division of Geology and Earth Resources Geologic Map GM-39, scale 1:250,000, 3 sheets, 36 p. text.

Tabor, R.W., 1994, Late Mesozoic and possible Early Tertiary accretion in western Washington State: The Helena-Haystack mélange and the Darrington–Devils Mountain fault zone: Geological Society of America Bulletin, v. 106, p. 217–232, doi:10.1130/0016-7606(1994)106<0217:LMAPET>2.3.CO;2.

Tabor, R.W., Waitt, R.B., Frizzell, V.A., Jr., Swanson, D.A., Byerly, G.R., and Bentley, R.D., 1982, Geologic Map of the Wenatchee 1:100,000 Quadrangle, Central Washington: U.S. Geological Survey Miscellaneous Investigations Series Map I-1311, scale 1:100,000, 1 sheet, 26 p. text.

Tabor, R.W., Frizzell, V.A., Jr., Vance, J.A., and Naeser, C.W., 1984, Ages and stratigraphy of Lower and Middle Tertiary sedimentary and volcanic rocks of the central Cascades: Application to the tectonic history of the Straight Creek fault: Geological Society of America Bulletin, v. 95, p. 26–44, doi:10.1130/0016-7606(1984)95<26:AASOLA>2.0.CO;2.

Tabor, R.W., Frizzell, V.A., Jr., Whetten, J.T., Waitt, R.B., Swanson, D.A., Byerly, G.R., Booth, D.B., Hetherington, M.J., and Zartman, R.E., 1987, Geologic Map of the Chelan 30′ × 60′ Quadrangle, Washington: U.S. Geological Survey Geologic Investigations Series I-1661, scale 1:100,000, 1 sheet, 33 p. text.

Tabor, R.W., Frizzell, V.A., Jr., Booth, D.B., Waitt, R.B., Whetten, J.T., and Zartman, R.E., 1993, Geologic Map of the Skykomish River 30′ × 60′ Quadrangle, Washington: U.S. Geological Survey Geologic Investigations Series I-1963, scale 1:100,000, 1 sheet, 42 p. text.

Tabor, R.W., Frizzell, V.A., Jr., Booth, D.B., and Waitt, R.B., 2000, Geologic Map of the Snoqualmie Pass 30′ × 60′ Minute Quadrangle, Washington: U.S. Geological Survey Geologic Investigations Series I-2538, scale 1:100,000, 1 sheet, 57 p. text.

Tabor, R.W., Booth, D.B., Vance, J.A., and Ford, A.B., 2002, Geologic Map of the Sauk River 30′ × 60′ Quadrangle, Washington: U.S. Geological Survey Geologic Investigations Series I-2592, scale 1:100,000, 2 sheets, 67 p. text.

Tabor, R.W., Haugerud, R.A., Hildreth, W., and Brown, E.H., 2003, Geologic Map of the Mount Baker 30′ × 60′ Quadrangle, Washington: U.S. Geological Survey Geologic Investigations Series I-2660, scale 1:100,000, 2 sheets, 73 p. text.

Taylor, S.B., Johnson, S.Y., Fraser, G.T., and Roberts, J.W., 1988, Sedimentation and tectonics of the Lower and Middle Eocene Swauk Formation in eastern Swauk basin, central Cascades, central Washington: Canadian Journal of Earth Sciences, v. 25, p. 1020–1036, doi:10.1139/e88-100.

Tepper, J.H., Clark, K., Asmerom, Y., and McIntosh, W., 2004, Eocene adakites in the Cascadia forearc: Implications for the position of the Kula-Farallon Ridge: Geological Society of America Abstracts with Programs, v. 36, no. 4, p. 69.

Thorkelson, D.J., and Breitsprecher, K., 2005, Partial melting of slab window margins: Genesis of adakitic magmas: Lithos, v. 79, p. 25–41, doi:10.1016/j.lithos.2004.04.049.

Trop, J.M., Ridgeway, K.D., and Spell, T.L., 2003, Sedimentary record of transpressional tectonics and ridge-subduction in the Tertiary Matanuska Valley–Talkeetna Mountains forearc basin, southern Alaska, *in* Sisson, V.B., Roeske, S.M., and Pavlis, T.L., eds., Geology of a Transpressional Orogen Developed During Ridge-Trench Interaction Along the North Pacific Margin: Geological Society of America Special Paper 371, p. 89–118, doi:10.1130/0-8137-2371-X.89.

Umhoefer, P.J., and Miller, R.B., 1996, Mid-Cretaceous thrusting in the southern Coast belt, British Columbia and Washington, after strike-slip fault reconstruction: Tectonics, v. 15, p. 545–565, doi:10.1029/95TC03498.

Vance, J.A., 1957, The Geology of the Sauk River Area in the Northern Cascades of Washington [Ph.D. thesis]: Seattle, Washington, University of Washington, 312 p.

Vine, J.D., 1969, Geology and Coal Resources of the Cumberland, Hobart, and Maple Valley Quadrangles, King County, Washington: U.S. Geological Survey Professional Paper 624, 67 p.

Walker, C.W., 1980, Geology and Energy Resources of the Roslyn–Cle Elum Area, Kittitas County, Washington: Washington Division of Geology and Earth Resources Open-File Report 80-1, scale 1:24,000, 1 sheet, 59 p. text.

Walsh, T.J., Korosec, M.A., Phillips, W.M., Logan, R.L., and Schasse, H.W., 1987, Geologic Map of Washington—Southwest Quadrant: Washington Division of Geology and Earth Resources Geologic Map GM-34, scale 1:250,000, 2 sheets, 28 p. text.

Wells, R.E., Engebretson, C.D., Snavely, P.D., Jr., and Coe, R.S., 1984, Cenozoic plate motions and the volcano-tectonic evolution of western Oregon and Washington: Tectonics, v. 3, p. 275–294, doi:10.1029/TC003i002p00275.

Wells, R.E., Weaver, C.S., and Blakely, R.J., 1998, Fore-arc migration in Cascadia and its neotectonic significance: Geology, v. 26, p. 759–762, doi:10.1130/0091-7613(1998)026<0759:FAMICA>2.3.CO;2.

Wells, R.E., Bukry, D., Friedman, R., Pyle, D., Duncan, R., Haeussler, P., and Wooden, J., 2014, Geologic history of Siletzia, a large igneous province in the Oregon and Washington Coast Range: Correlation to the geomagnetic polarity time scale and implications for a long-lived Yellowstone hotspot: Geosphere, v. 10, p. 692–719, doi:10.1130/GES01018.1.

Wendt, I., and Carl, C., 1991, The statistical distribution of the mean squared weighted deviation: Chemical Geology, v. 86, p. 275–285, doi:10.1016/0168-9622(91)90010-T.

Wiebe, R.A., 1963, The Geology of Mt. Pilchuck [M.S. thesis]: Seattle, Washington, University of Washington, 52 p.

Wintzer, N.E., 2012, Deformational episodes recorded in the Skagit gneiss complex, north Cascades, Washington, USA: Journal of Structural Geology, v. 42, p. 127–139, doi:10.1016/j.jsg.2012.06.004.

Wyld, S.J., Umhoefer, P.J., and Wright, J.E., 2006, Reconstructing northern Cordilleran terranes along known Cretaceous and Cenozoic strike-slip faults: Implications for the Baja–British Columbia hypothesis and other models, *in* Haggart, J.W., Enkin, R.J., and Monger, J.W.H., eds., Paleogeography of the North American Cordillera: Evidence For and Against Large-Scale Displacements: Geological Association of Canada Special Paper 46, p. 277–298.

Yeats, R.S., and Engels, J.C., 1971, Potassium-Argon Ages of Plutons in the Skykomish-Stillaguamish Areas, North Cascades, Washington: U.S. Geological Survey Professional Paper 750-D, p. D34–D38.

Science Editor: Christian Koeberl
Associate Editor: Stephen T. Johnston

Manuscript Received 10 April 2015
Revised Manuscript Received 11 July 2015
Manuscript Accepted 3 September 2015

Printed in the USA

TABLE DR1: CA-IDTIMS U-Pb ZIRCON GEOCHRONOLOGY RESULTS

Frac.	Dates $^{206}Pb/^{238}U^{*}$	2σ abs.	$^{207}Pb/^{235}U^{\dagger}$	2σ abs.	$^{207}Pb/^{206}Pb^{\dagger}$	2σ abs.	% Disc.[§]	Corr. Coef.	Composition Th/U[#]	Pb_c (pg)[**]	Pb*/Pb_c[††]	Isotopic Ratios $^{206}Pb/^{204}Pb$[§§]	$^{208}Pb/^{206}Pb$[##]	$^{206}Pb/^{238}U^{*,\#\#}$	2σ %	$^{207}Pb/^{235}U^{\#\#}$	2σ %	$^{207}Pb/^{206}Pb^{*,\#\#}$	2σ %
NC-203																			
z1	57.23	0.32	57.7	4.7	83	190	31.09	0.312	0.43	0.25	2	157	0.138	0.008917	0.57	0.0585	8.3	0.047615	8.1
z2	57.083	0.060	57.15	0.67	63	28	9.69	0.445	0.74	0.20	20	1100	0.238	0.008894	0.11	0.05789	1.2	0.047230	1.2
z3	56.98	0.10	55.4	1.4	-9	59	700.88	0.387	0.38	0.22	8	517	0.121	0.008878	0.18	0.0560	2.5	0.045810	2.5
z4	57.03	0.17	56.9	2.3	54	98	-5.96	0.293	0.47	0.33	5	301	0.150	0.008885	0.30	0.0576	4.2	0.047035	4.1
z5	56.86	0.16	56.3	2.1	34	89	-64.59	0.381	0.50	0.29	5	341	0.161	0.008860	0.28	0.0570	3.8	0.046659	3.7
zl	56.70	0.12	56.8	1.2	64	47	12.00	0.482	0.45	0.31	11	646	0.146	0.008835	0.21	0.0575	2.1	0.047244	2.0
zm	57.10	0.10	55.6	1.4	-6	60	1099.13	0.473	0.34	0.38	10	610	0.109	0.008896	0.18	0.0563	2.6	0.045880	2.5
zn	56.973	0.049	56.92	0.48	58	20	2.63	0.308	0.59	0.30	26	1514	0.188	0.008877	0.086	0.05766	0.87	0.047132	0.85
zo	56.855	0.069	56.82	0.57	59	23	4.22	0.545	0.35	0.44	22	1385	0.112	0.008859	0.12	0.05755	1.0	0.047140	0.98
zp	57.073	0.074	57.13	0.81	63	34	10.13	0.383	0.46	0.60	14	829	0.148	0.008893	0.13	0.05788	1.5	0.047226	1.4
zq	57.15	0.21	59.3	2.9	149	120	61.70	0.320	0.58	0.91	4	240	0.186	0.008905	0.37	0.0601	5.1	0.048972	5.0
zu	57.57	0.22	58.4	3.1	97	120	40.95	0.329	0.59	1.13	4	229	0.189	0.008971	0.38	0.0592	5.4	0.047911	5.3
zv	56.92	0.16	57.5	2.2	84	92	32.08	0.351	0.36	0.57	5	309	0.114	0.008869	0.29	0.0582	4.0	0.047627	3.9
zw	57.023	0.083	57.69	0.97	89	40	36.12	0.367	0.49	0.49	11	681	0.157	0.008885	0.15	0.0585	1.7	0.047741	1.7
zy	56.88	0.40	56.1	5.6	28	240	-106.45	0.405	0.30	0.32	2	138	0.098	0.008862	0.71	0.0568	10	0.046517	10
zz	56.85	0.18	57.1	2.5	71	100	20.29	0.392	0.46	0.41	5	288	0.147	0.008858	0.32	0.0578	4.5	0.047381	4.3
NC-MPE-016																			
z5-1	67.894	0.038	67.94	0.13	73.1	4.1	7.23	0.538	0.31	0.42	150	9341	0.098	0.010588	0.056	0.06920	0.20	0.047427	0.17
z71-1	59.919	0.098	60.7	1.3	94	52	36.46	0.316	0.40	1.03	8	518	0.127	0.009338	0.16	0.0616	2.2	0.047843	2.2
z81-1	69.14	0.16	67.3	2.2	7	78	-845.14	0.264	0.27	0.51	6	404	0.087	0.010784	0.24	0.0686	3.3	0.046141	3.3
NC-190																			
z1	51.313	0.073	51.24	0.79	52	37	2.42	0.370	0.34	0.57	12	750	0.108	0.007992	0.14	0.05176	1.6	0.046998	1.5
z3	51.40	0.14	52.1	1.6	88	74	41.82	0.248	0.44	0.68	6	389	0.141	0.008006	0.27	0.0526	3.2	0.047712	3.1
z4	52.262	0.082	54.22	0.84	146	36	64.28	0.380	0.35	0.40	12	760	0.113	0.00814	0.16	0.05485	1.6	0.048895	1.5
z5	51.291	0.08	51.71	0.79	75	37	31.94	0.239	0.48	0.97	13	784	0.155	0.007988	0.16	0.05224	1.6	0.047454	1.5
z6	51.78	0.13	52.6	1.5	95	67	45.67	0.396	0.33	0.96	7	438	0.105	0.008065	0.26	0.0532	2.9	0.047849	2.8
z7	51.63	0.13	52.1	1.8	76	82	32.27	0.371	0.27	0.65	5	352	0.087	0.008041	0.26	0.0526	3.5	0.047464	3.5
z8	51.364	0.047	51.65	0.51	70	24	26.26	0.281	0.31	0.68	18	1130	0.099	0.008	0.092	0.05219	1.0	0.047334	1.0
z9	51.46	0.14	50.9	1.9	28	91	-83.94	0.331	0.22	0.58	5	324	0.072	0.008015	0.28	0.0514	3.9	0.046514	3.8
z13	51.414	0.061	51.41	0.66	55	31	7.49	0.214	0.32	0.47	15	925	0.102	0.008008	0.12	0.05193	1.3	0.047056	1.3
z14	51.482	0.082	52.15	0.92	87	42	41.15	0.390	0.26	0.38	11	706	0.084	0.008018	0.16	0.05270	1.8	0.047688	1.8
z15	51.84	0.11	52.5	1.4	89	62	41.96	0.350	0.27	0.39	7	451	0.087	0.008074	0.21	0.0531	2.7	0.047726	2.6
NC-MPE-358B																			
z1	76.09	0.11	75.5	1.3	61	41	-24.04	0.379	0.37	0.55	11	700	0.118	0.011874	0.14	0.0772	1.8	0.047201	1.7
z2	52.95	0.33	52.6	5.0	42	230	-26.02	0.331	0.88	0.27	2	142	0.282	0.008248	0.63	0.0532	9.8	0.046813	9.6
z3	51.548	0.042	51.51	0.40	54	18	5.39	0.383	0.28	0.41	25	1593	0.089	0.008028	0.081	0.05204	0.80	0.047033	0.77
z4	89.951	0.093	89.82	0.93	89	25	-1.13	0.305	0.26	0.24	19	1198	0.083	0.014051	0.1	0.0925	1.1	0.047759	1.1
z5	90.97	0.18	89.8	1.8	62	50	-46.68	0.328	0.29	0.29	10	655	0.091	0.014211	0.2	0.0925	2.1	0.047222	2.1
z6	90.156	0.060	90.36	0.28	98.4	6.8	8.52	0.608	0.13	0.35	72	4719	0.042	0.014084	0.067	0.09307	0.32	0.047950	0.29
z7	92.52	0.14	92.2	1.6	87	42	-5.86	0.53	0.27	0.37	11	738	0.087	0.014456	0.15	0.0951	1.9	0.047729	1.8
z8	51.43	0.11	52.1	1.5	88	66	41.99	0.324	0.21	0.66	6	421	0.069	0.008010	0.21	0.0527	2.9	0.047710	2.8
z9	89.71	0.20	89.8	2.6	95	70	5.31	0.291	0.25	0.33	6	411	0.080	0.014014	0.22	0.0925	3	0.047875	3.0
z10	89.312	0.092	89.4	1.0	95	28	6.35	0.339	0.17	0.57	15	975	0.054	0.013951	0.1	0.0921	1.2	0.047886	1.2
z11	89.87	0.47	89.5	6.3	83	170	-7.64	0.33	0.30	0.23	3	184	0.096	0.014039	0.52	0.0922	7.3	0.047650	7.1
z13	93.03	0.37	103.9	4.6	363	100	74.38	0.362	0.15	0.21	4	247	0.047	0.014537	0.4	0.1077	4.7	0.053765	4.5
z14	51.496	0.039	51.16	0.33	40	15	-27.89	0.418	0.18	0.23	31	1998	0.056	0.008020	0.076	0.05168	0.66	0.046751	0.63

NC-MPE-419B																		
z1	51.397	0.091	51.5	1.2	61	56	15.93	0.324	0.43	0.49	8	492	0.138	0.008005	0.18	0.0520	2.4	0.047170	2.4
z3	51.287	0.070	51.45	0.87	63	40	19.36	0.395	0.39	0.31	12	732	0.125	0.007988	0.14	0.05198	1.7	0.047217	1.7
z4	51.315	0.089	50.60	0.87	21	40	-142.13	0.468	0.34	0.44	14	877	0.109	0.007992	0.17	0.05109	1.8	0.046387	1.7
z6	51.277	0.039	50.93	0.36	39	17	-30.31	0.3	0.32	0.25	29	1840	0.103	0.007986	0.076	0.05144	0.72	0.046738	0.70
z7	51.332	0.041	51.35	0.30	57	14	9.49	0.431	0.31	0.25	33	2054	0.101	0.007995	0.079	0.05187	0.60	0.047078	0.57
z9	51.833	0.092	50.5	1.6	-8	79	725.23	0.393	0.36	0.32	7	468	0.115	0.008073	0.18	0.0510	3.3	0.045825	3.3
NC-MPE-420B																		
z1	49.178	0.035	49.23	0.29	56	14	12.61	0.301	0.53	0.20	39	2278	0.168	0.007658	0.072	0.04968	0.61	0.047074	0.59
z3	48.999	0.029	49.044	0.081	55.9	3.7	12.57	0.451	0.31	0.22	164	10241	0.100	0.007630	0.059	0.049486	0.17	0.047060	0.15
z5	49.040	0.035	49.07	0.25	55	12	11.00	0.329	0.50	0.20	39	2328	0.160	0.007636	0.072	0.04952	0.53	0.047049	0.51
NC-MPE-421																		
z1	50.07	0.24	52.4	3.4	166	150	69.82	0.298	0.38	0.91	3	179	0.123	0.007798	0.48	0.0530	6.7	0.049304	6.5
z2	50.21	0.45	52.6	6.6	167	300	70.06	0.309	0.51	0.76	1	103	0.162	0.007819	0.90	0.0532	13	0.049346	13
z3	50.30	0.61	54.2	9.0	236	390	78.74	0.328	0.47	1.14	1	84	0.151	0.007833	1.2	0.0549	17	0.050827	17
z4	49.99	0.26	51.8	3.7	139	170	64.03	0.301	0.45	1.50	2	166	0.144	0.007784	0.52	0.0523	7.4	0.048743	7.3
z5	49.85	0.12	47.2	1.6	-81	85	161.08	0.388	0.34	0.22	6	395	0.110	0.007764	0.24	0.0476	3.5	0.044462	3.5
z7	49.84	0.13	48.6	1.7	-9	83	651.78	0.435	0.43	0.24	6	389	0.138	0.007761	0.26	0.0490	3.5	0.045810	3.4
z9	50.14	0.11	51.0	1.5	94	69	46.71	0.471	0.39	0.19	7	459	0.124	0.007809	0.23	0.0515	3.0	0.047824	2.9
z10	50.001	0.09	50.7	1.2	88	58	43.04	0.324	0.38	0.25	8	479	0.122	0.007787	0.18	0.0512	2.5	0.047696	2.4
NC-MPE-436																		
z1	49.716	0.051	49.47	0.38	42	18	-17.59	0.340	0.31	0.30	28	1784	0.099	0.007742	0.10	0.04993	0.78	0.046792	0.75
z2	49.82	0.12	49.9	1.7	60	81	17.09	0.301	0.41	0.83	5	348	0.132	0.007759	0.24	0.0504	3.5	0.047146	3.4
z3	49.62	0.15	49.8	2.1	65	100	23.82	0.293	0.52	0.89	4	274	0.166	0.007728	0.30	0.0503	4.4	0.047249	4.3
z7	49.677	0.048	49.43	0.47	42	23	-17.91	0.167	0.25	0.25	20	1306	0.081	0.007736	0.098	0.04988	0.97	0.046787	0.96
z9	49.756	0.075	49.60	0.89	46	42	-8.20	0.443	0.68	0.22	13	748	0.218	0.007748	0.15	0.05006	1.8	0.046878	1.8
z11	49.746	0.053	49.93	0.34	63	16	21.67	0.445	0.25	0.21	32	2054	0.080	0.007747	0.11	0.05040	0.70	0.047207	0.66
z12	49.661	0.064	49.21	0.50	32	23	-54.62	0.508	0.20	0.28	25	1603	0.065	0.007733	0.13	0.04966	1.0	0.046590	0.98
NC-MPE-356																		
z5	49.395	0.063	49.48	0.83	58	40	15.26	0.241	0.47	0.40	11	695	0.151	0.007692	0.13	0.04994	1.7	0.047112	1.7
z7	49.55	0.11	49.8	1.6	66	75	24.77	0.343	0.42	0.52	6	383	0.135	0.007716	0.22	0.0503	3.2	0.047260	3.2
z8	49.372	0.077	49.9	1.0	81	48	38.85	0.381	0.41	0.34	10	594	0.132	0.007688	0.16	0.0504	2.1	0.047555	2.0
z9	49.35	0.16	49.0	2.2	35	110	-40.03	0.344	0.51	0.32	4	275	0.162	0.007685	0.32	0.0494	4.6	0.046661	4.5
z10	49.285	0.052	48.77	0.65	28	32	-76.31	0.343	0.49	0.30	16	953	0.155	0.007675	0.11	0.04920	1.4	0.046519	1.3
z11	49.38	0.13	48.5	1.7	12	85	-311.81	0.347	0.44	0.36	6	356	0.139	0.007689	0.26	0.0490	3.6	0.046210	3.5
ED072413-147																		
z1	49.24	0.17	50.7	2.4	123	110	59.91	0.306	0.46	0.90	4	243	0.148	0.007667	0.34	0.0511	4.9	0.048409	4.8
z2	49.17	0.14	49.8	2.0	83	94	41.11	0.308	0.38	1.11	5	296	0.120	0.007656	0.28	0.0502	4.0	0.047608	4.0
z3	49.147	0.058	49.64	0.80	78	39	37.24	0.258	0.41	0.44	12	713	0.131	0.007653	0.12	0.05011	1.7	0.047506	1.6
z4	85.3	1.0	91	14	243	360	64.95	0.303	0.46	1.12	1	84	0.148	0.013326	1.2	0.094	16	0.051021	16
z5	49.08	0.13	49.9	1.9	92	92	46.94	0.306	0.31	0.63	5	310	0.099	0.007642	0.28	0.0503	3.9	0.047786	3.9
z6	49.32	0.24	51.2	3.5	143	160	65.54	0.295	0.47	0.62	3	176	0.151	0.007680	0.49	0.0517	6.9	0.048828	6.8
z7	49.119	0.089	49.5	1.2	70	58	30.14	0.347	0.55	0.51	8	491	0.175	0.007649	0.18	0.0499	2.5	0.047352	2.4
z8	51.42	0.77	60	11	429	420	88.04	0.327	0.45	0.95	1	69	0.143	0.008008	1.5	0.061	19	0.055347	19
NC-MPE-359																		
z1	48.987	0.091	48.9	1.3	50	62	3.08	0.351	0.49	0.44	8	466	0.156	0.007628	0.19	0.0494	2.6	0.046959	2.6
z2	48.95	0.24	49.7	3.5	88	170	44.70	0.301	0.41	0.63	3	175	0.133	0.007622	0.49	0.0501	7.1	0.047710	7
z3	66.34	0.87	75	12	359	380	81.53	0.281	0.39	5.65	1	75	0.123	0.010345	1.3	0.076	17	0.053652	17
z4	49.13	0.74	54	11	270	470	81.85	0.312	0.61	1.88	1	68	0.196	0.007651	1.5	0.054	21	0.051590	20
z5	49.18	0.24	51.2	3.5	149	160	67.16	0.307	0.33	1.55	3	173	0.104	0.007658	0.50	0.0517	7.1	0.048960	6.9
z6	49.13	0.22	50.3	3.2	110	150	55.41	0.332	0.49	0.24	3	206	0.156	0.007651	0.44	0.0508	6.4	0.048152	6.3
z7	49.10	0.29	50.0	4.1	97	190	49.30	0.439	0.40	0.36	2	168	0.129	0.007645	0.59	0.0504	8.4	0.047878	8.2

NC-MPE-359 (Cont'd)																		
z9	48.95	0.1	48.8	1.4	47	70	-4.96	0.322	0.53	0.51	7	407	0.169	0.007623	0.21	0.0493	3	0.046884	2.9
z10	48.931	0.048	48.85	0.54	50	26	1.37	0.385	0.38	0.39	18	1090	0.123	0.007619	0.099	0.04929	1.1	0.046937	1.1
ED062313-035																			
z1	48.548	0.034	48.57	0.22	54	11	10.56	0.295	0.36	0.61	45	2784	0.115	0.007559	0.071	0.04899	0.46	0.047027	0.44
z2	48.76	0.21	50.1	3.1	118	140	58.64	0.303	0.35	1.58	3	195	0.113	0.007592	0.44	0.0505	6.3	0.048302	6.1
z3	48.79	0.26	49.8	3.7	104	180	53.30	0.363	0.35	0.35	2	171	0.112	0.007597	0.54	0.0503	7.6	0.048029	7.5
z4	48.494	0.034	48.33	0.34	45	17	-7.88	0.203	0.45	0.66	31	1855	0.145	0.007551	0.070	0.04875	0.72	0.046847	0.70
z5	48.662	0.044	48.77	0.50	59	25	17.62	0.333	0.38	0.52	18	1130	0.122	0.007577	0.092	0.04921	1.1	0.047122	1.0
z6	48.525	0.032	48.65	0.14	59.5	6.6	18.58	0.349	0.37	0.43	74	4529	0.117	0.007556	0.067	0.04908	0.29	0.047132	0.28
z7	48.510	0.032	48.46	0.34	51	17	4.93	0.208	0.36	0.36	30	1839	0.116	0.007553	0.066	0.04889	0.71	0.046963	0.70
z8	48.541	0.051	48.44	0.62	48	30	-0.71	0.360	0.38	0.47	15	953	0.123	0.007558	0.10	0.04886	1.3	0.046908	1.3
z9	48.531	0.061	48.58	0.79	56	39	12.88	0.330	0.36	0.40	11	723	0.115	0.007557	0.13	0.04901	1.7	0.047055	1.6
NC-MPE-365B																			
z1	48.290	0.046	48.45	0.45	61	22	20.36	0.432	0.56	0.19	24	1392	0.180	0.007519	0.095	0.04887	0.94	0.047159	0.91
z2	48.376	0.036	48.53	0.21	60.7	9.9	20.49	0.351	0.49	0.19	55	3277	0.155	0.007533	0.075	0.04896	0.43	0.047161	0.41
z3	48.41	0.48	49.0	6.9	83	340	42.03	0.321	0.46	0.67	1	97	0.147	0.007538	1.0	0.0495	14	0.047611	14
z4	163.00	0.87	160	11	115	170	-41.18	0.299	0.53	0.52	3	173	0.170	0.025608	0.54	0.171	7.4	0.048325	7.3
z5	68.72	0.39	69.6	5.2	104	180	33.96	0.375	0.51	0.37	3	168	0.163	0.010717	0.57	0.0710	7.8	0.048054	7.6
z6	67.28	0.19	69.0	2.6	132	88	49.15	0.321	0.67	0.44	5	314	0.214	0.010492	0.28	0.0703	3.8	0.048636	3.7
z7	67.82	0.58	70.0	8	148	270	54.12	0.361	0.57	0.30	2	118	0.181	0.010576	0.86	0.0714	12	0.048955	12
STC62-1																			
z2	48.191	0.048	48.35	0.38	61	19	20.56	0.180	0.59	0.41	28	1656	0.190	0.007504	0.10	0.04877	0.80	0.047161	0.79
z3	48.172	0.062	48.06	0.72	47	35	-2.19	0.425	0.38	0.34	13	830	0.120	0.007501	0.13	0.04847	1.5	0.046886	1.5
z4	48.176	0.048	48.06	0.60	47	30	-3.25	0.128	0.49	0.38	16	969	0.155	0.007501	0.10	0.04847	1.3	0.046881	1.3
z6	68.397	0.057	68.28	0.37	68	13	-1.19	0.433	0.40	0.59	39	2361	0.126	0.010667	0.083	0.06956	0.56	0.047318	0.53
z7	48.201	0.059	48.37	0.82	61	41	21.76	0.254	0.43	0.58	11	703	0.138	0.007505	0.12	0.04879	1.7	0.047173	1.7
z8	48.22	0.12	48.6	1.7	72	83	32.91	0.335	0.56	0.67	6	339	0.179	0.007508	0.26	0.0490	3.6	0.047382	3.5
NMNC366-2																			
z1	47.967	0.048	48.07	0.52	58	26	17.33	0.375	0.47	0.88	18	1108	0.150	0.007469	0.1	0.04848	1.1	0.047104	1.1
z2	47.994	0.092	48.1	1.3	57	63	16.06	0.362	0.49	0.98	7	460	0.156	0.007473	0.19	0.0485	2.7	0.047088	2.6
z7	47.984	0.064	48.39	0.77	73	38	34.24	0.375	0.49	0.55	12	756	0.156	0.007471	0.13	0.04881	1.6	0.047400	1.6
z10	47.995	0.038	48.01	0.36	53	17	9.77	0.376	0.52	0.56	27	1619	0.166	0.007473	0.08	0.04842	0.76	0.047010	0.73
z11	48.012	0.043	48.16	0.37	60	18	20.45	0.289	0.43	0.35	25	1514	0.137	0.007476	0.089	0.04858	0.78	0.047148	0.76
z12	47.952	0.036	48.03	0.25	56	12	14.95	0.323	0.60	0.52	40	2288	0.193	0.007466	0.075	0.04844	0.54	0.047076	0.52
ED070113-063																			
z39	47.879	0.040	48.05	0.14	61.4	7	22.13	0.170	0.43	0.38	98	5892	0.136	0.007455	0.083	0.04846	0.30	0.04717	0.29
z69	47.847	0.085	47.1	1.1	16	54	-192.31	0.411	0.46	0.55	10	637	0.146	0.007450	0.18	0.04750	2.3	0.046292	2.2
ED071613-127																			
z08	47.364	0.074	47.06	0.70	36	34	-30.04	0.647	0.48	0.30	15	929	0.152	0.007374	0.16	0.04744	1.5	0.046679	1.4
z99	46.902	0.076	44.29	0.81	-90	44	151.91	0.377	0.31	0.32	10	655	0.099	0.007302	0.16	0.04458	1.9	0.044297	1.8
NC-MPE-015																			
z4-5	48.875	0.065	48.90	0.11	55.0	3.9	11.34	0.687	0.28	0.50	161	10136	0.088	0.007611	0.13	0.04934	0.22	0.047041	0.16
z6-8	49.513	0.029	49.496	0.080	52.4	3.4	5.69	0.578	0.82	0.25	325	17675	0.263	0.007710	0.059	0.049954	0.17	0.047011	0.14
z7-8a	49.18	0.91	58	14	447	530	89.01	0.398	0.45	0.45	1	62	0.145	0.007658	1.9	0.059	24	0.055782	24
z7-8b	48.80	0.11	48.0	1.6	14	79	-241.13	0.317	0.31	0.35	6	370	0.100	0.007600	0.23	0.0484	3.4	0.046249	3.3
NC-MPE-014																			
z3-1	49.010	0.029	49.019	0.089	54.1	3.8	9.64	0.578	0.33	0.36	142	8783	0.107	0.007632	0.059	0.049460	0.19	0.047026	0.16
z13-1	50.132	0.040	50.20	0.31	57	15	11.63	0.248	0.93	0.34	45	2393	0.298	0.007807	0.080	0.05068	0.62	0.047099	0.61
z88-1	47.580	0.028	47.74	0.14	59.8	6.6	20.60	0.359	0.70	0.29	99	5576	0.223	0.007408	0.060	0.04814	0.29	0.047149	0.27

NC-MPE-014 (Cont'd)																		
z93-1	49.258	0.047	49.59	0.60	69	29	29.20	0.278	0.66	0.72	17	996	0.213	0.007670	0.095	0.05005	1.2	0.047342	1.2
NC-MPE-020																		
z3	45.889	0.045	45.85	0.49	48	25	5.31	0.307	0.53	0.86	18	1089	0.170	0.007144	0.099	0.04619	1.1	0.046914	1.1
z4	45.911	0.063	46.28	0.61	70	31	34.95	0.238	0.37	0.98	14	879	0.117	0.007147	0.14	0.04664	1.3	0.047344	1.3
z5	45.932	0.043	45.82	0.38	45	20	-2.95	0.293	0.55	1.03	23	1376	0.175	0.007151	0.094	0.04616	0.86	0.046839	0.83
z6	45.907	0.032	46.09	0.21	60	11	24.07	0.248	0.58	0.39	44	2566	0.186	0.007147	0.070	0.04644	0.47	0.047152	0.46
NC-MPE-417A																		
z1	25.613	0.023	25.58	0.13	32	12	20.69	0.284	0.24	0.91	37	2363	0.078	0.003981	0.090	0.02552	0.53	0.046506	0.51
z2	25.625	0.037	25.95	0.50	66	45	61.15	0.340	0.20	0.82	9	606	0.063	0.003983	0.14	0.02589	2.0	0.047160	1.9
z3	25.662	0.083	26.1	1.2	74	110	65.29	0.300	0.47	1.25	4	253	0.151	0.003989	0.32	0.0260	4.8	0.047338	4.7
z4	25.587	0.027	25.45	0.36	21	33	-22.19	0.318	0.47	0.94	14	867	0.152	0.003977	0.11	0.02538	1.4	0.046303	1.4
z5	25.685	0.094	26.6	1.4	116	120	77.90	0.299	0.39	0.75	3	225	0.126	0.003992	0.37	0.0265	5.3	0.048183	5.2
z6	25.616	0.039	25.91	0.53	62	49	59.15	0.329	0.19	0.91	8	564	0.060	0.003982	0.15	0.02584	2.1	0.047095	2.0
NC-MPE-418																		
z1	24.234	0.025	24.22	0.22	31	22	23.33	0.280	0.45	0.22	30	1793	0.145	0.003766	0.10	0.02414	0.93	0.046498	0.90
z2	24.206	0.018	24.19	0.14	32	14	25.35	0.242	0.36	0.17	39	2392	0.117	0.003762	0.073	0.02411	0.58	0.046507	0.56
z3	24.217	0.015	24.31	0.12	43	11	43.82	0.391	0.35	0.27	41	2527	0.112	0.003764	0.064	0.02423	0.49	0.046713	0.47

* Corrected for initial Th/U disequilibrium using radiogenic ^{208}Pb and $Th/U_{[Magma]}$=2.8±0.5.
† Isotopic dates calculated using the decay constants λ238 = 1.55125E-10 and λ235 = 9.8485E-10 (Jaffey et al. 1971).
§ % discordance = 100 - (100 * ($^{206}Pb/^{238}U$ date) / ($^{207}Pb/^{206}Pb$ date))
# Th contents calculated from radiogenic ^{208}Pb and the $^{207}Pb/^{206}Pb$ date of the sample, assuming concordance between U-Th and Pb systems.
** Total mass of common Pb.
†† Ratio of radiogenic Pb (including ^{208}Pb) to common Pb.
§§ Measured ratio corrected for fractionation and spike contribution only.
Measured ratios corrected for fractionation, tracer and blank.

FIGURE DR1: CA-IDTIMS U-Pb zircon geochronology results presented as traditional concordia diagrams.

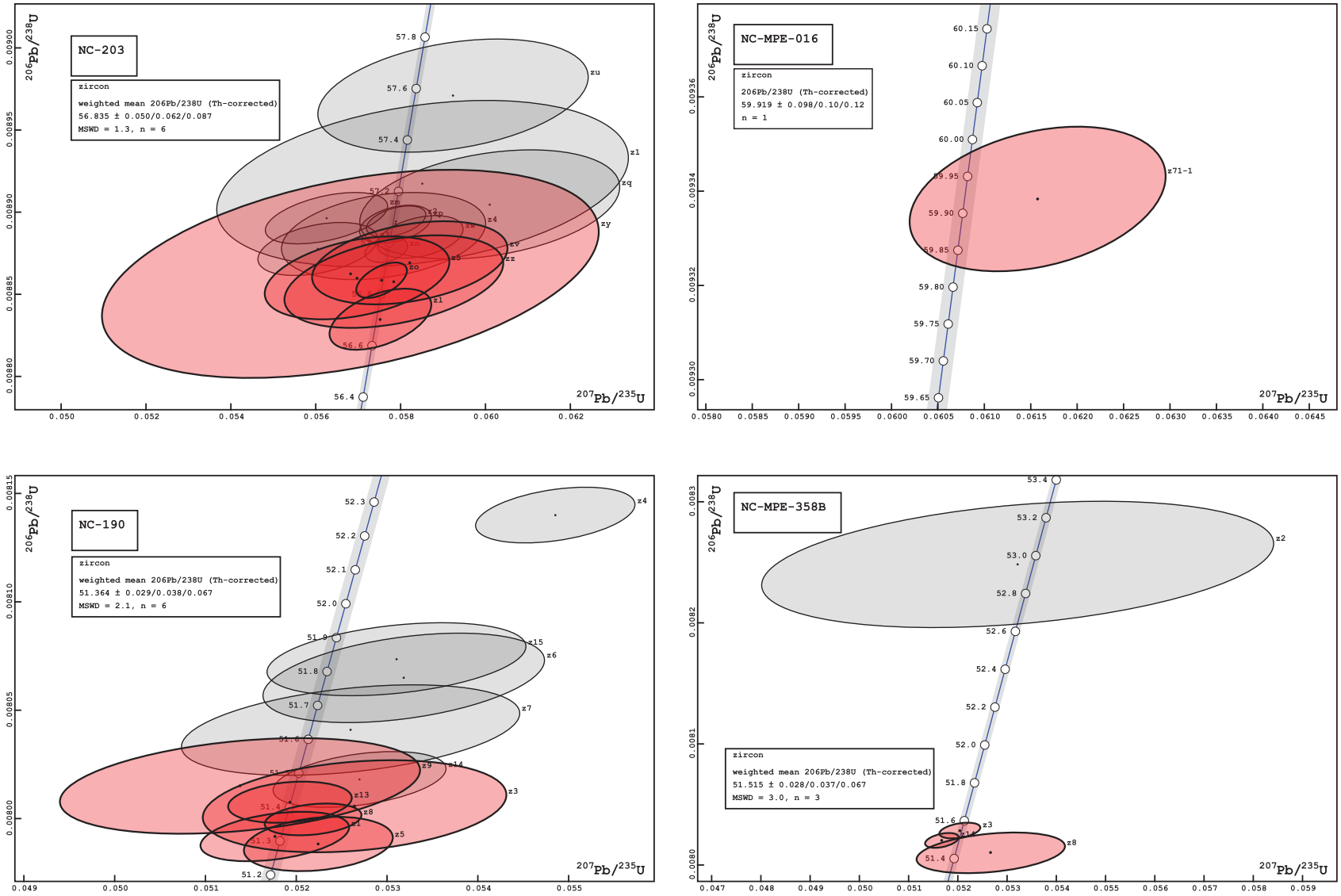

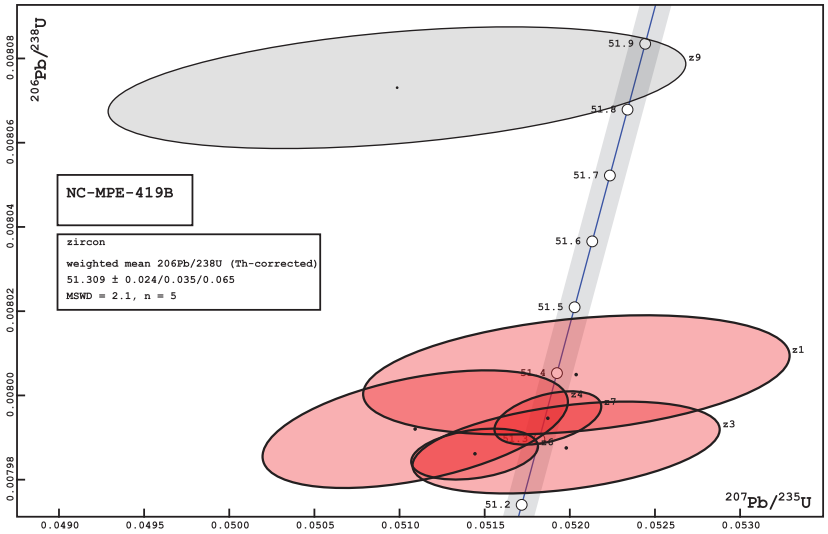
NC-MPE-419B
zircon
weighted mean 206Pb/238U (Th-corrected)
51.309 ± 0.024/0.035/0.065
MSWD = 2.1, n = 5
206Pb/238U
207Pb/235U

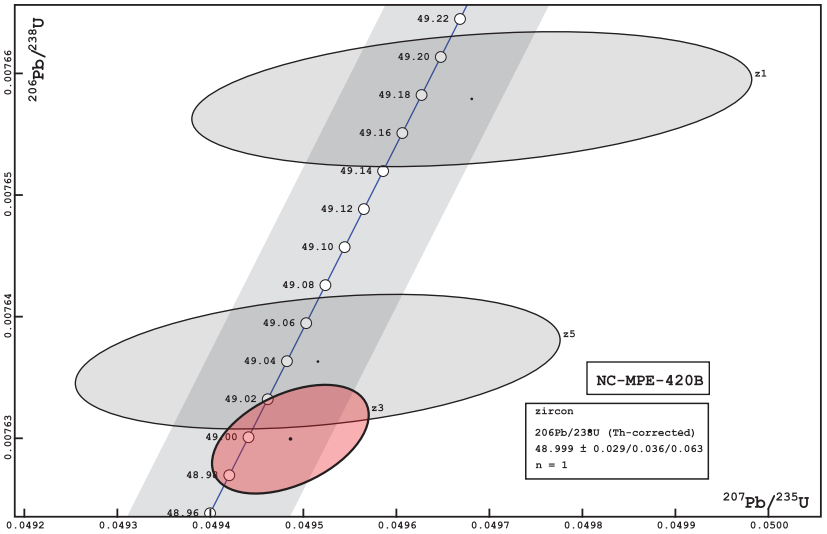
NC-MPE-420B
zircon
206Pb/238U (Th-corrected)
48.999 ± 0.029/0.036/0.063
n = 1
206Pb/238U
207Pb/235U

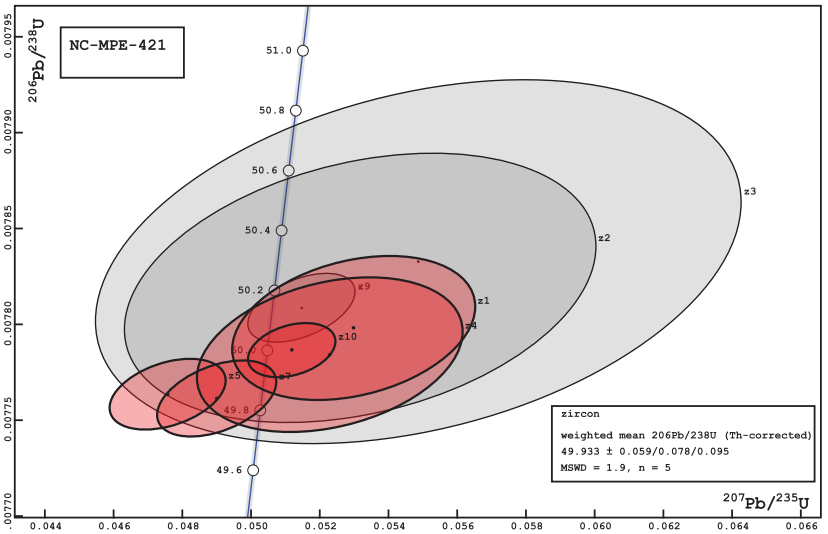
NC-MPE-421
zircon
weighted mean 206Pb/238U (Th-corrected)
49.933 ± 0.059/0.078/0.095
MSWD = 1.9, n = 5
206Pb/238U
207Pb/235U

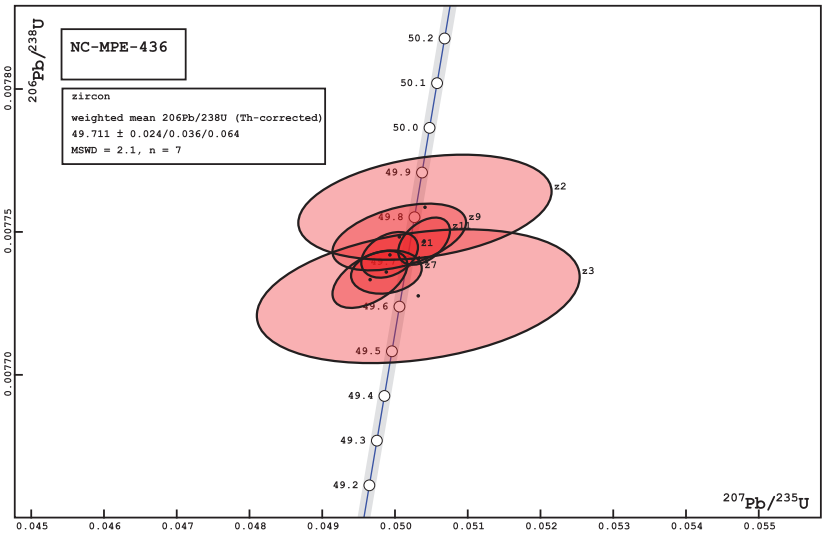
NC-MPE-436
zircon
weighted mean 206Pb/238U (Th-corrected)
49.711 ± 0.024/0.036/0.064
MSWD = 2.1, n = 7
206Pb/238U
207Pb/235U

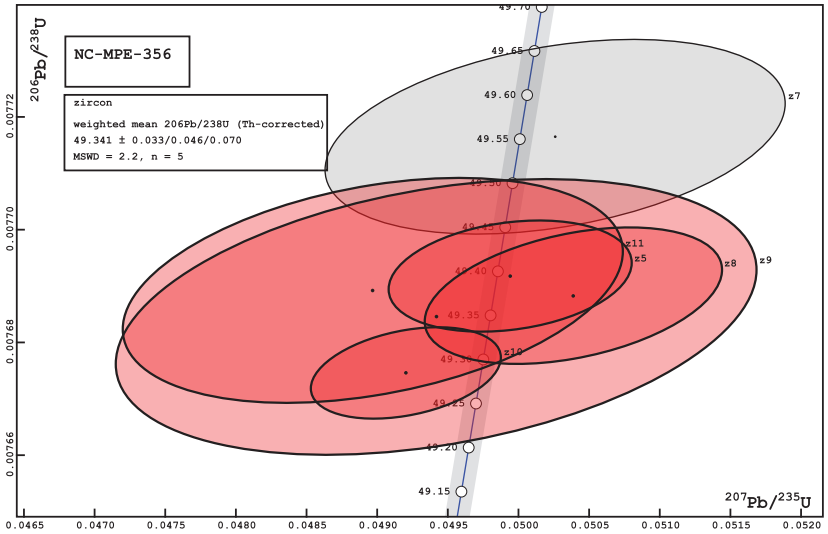
NC-MPE-356
zircon
weighted mean 206Pb/238U (Th-corrected)
49.341 ± 0.033/0.046/0.070
MSWD = 2.2, n = 5
206Pb/238U
207Pb/235U

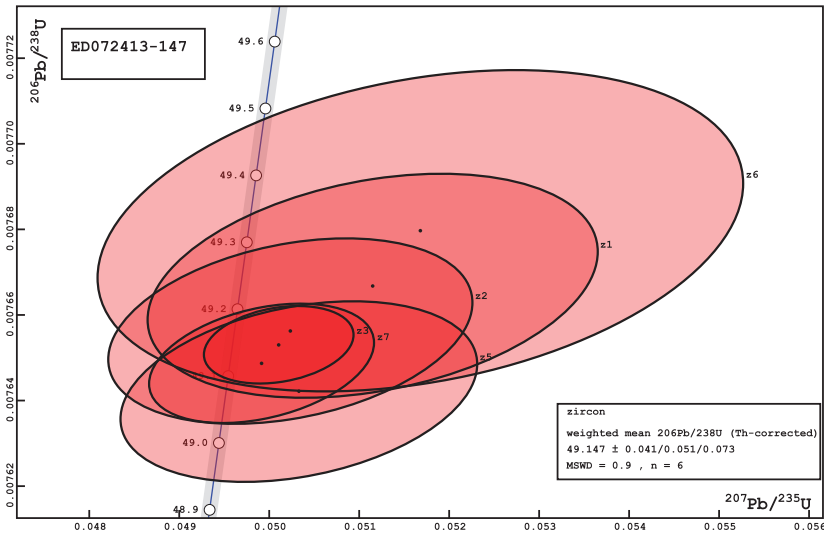
ED072413-147
zircon
weighted mean 206Pb/238U (Th-corrected)
49.147 ± 0.041/0.051/0.073
MSWD = 0.9 , n = 6
206Pb/238U
207Pb/235U

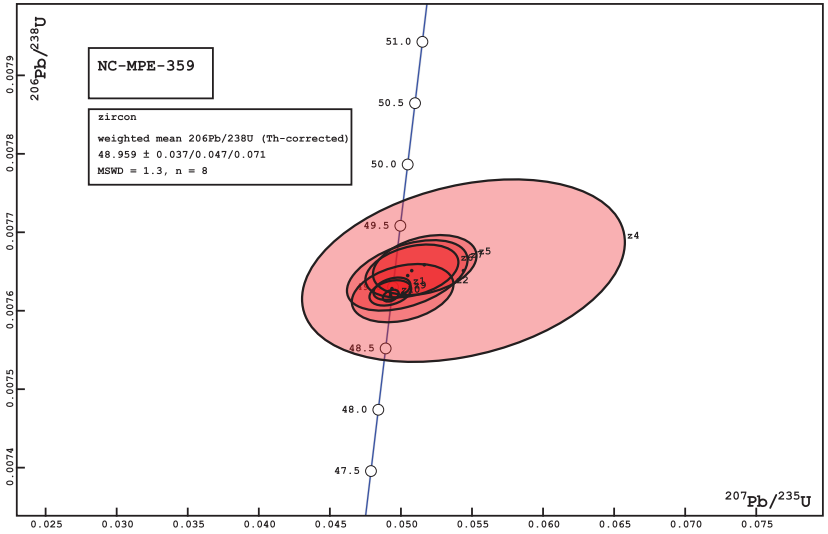
NC-MPE-359
zircon
weighted mean 206Pb/238U (Th-corrected)
48.959 ± 0.037/0.047/0.071
MSWD = 1.3, n = 8
206Pb/238U
207Pb/235U

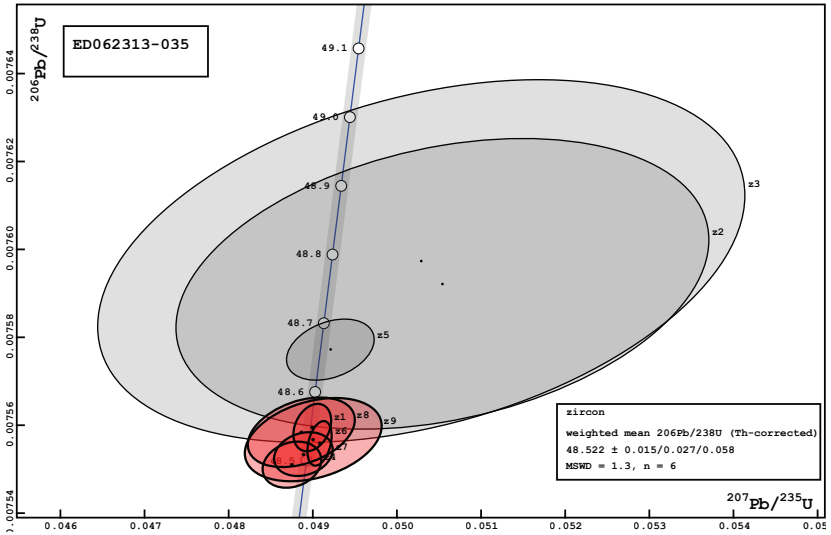
ED062313-035
zircon
weighted mean 206Pb/238U (Th-corrected)
48.522 ± 0.015/0.027/0.058
MSWD = 1.3, n = 6
206Pb/238U
207Pb/235U

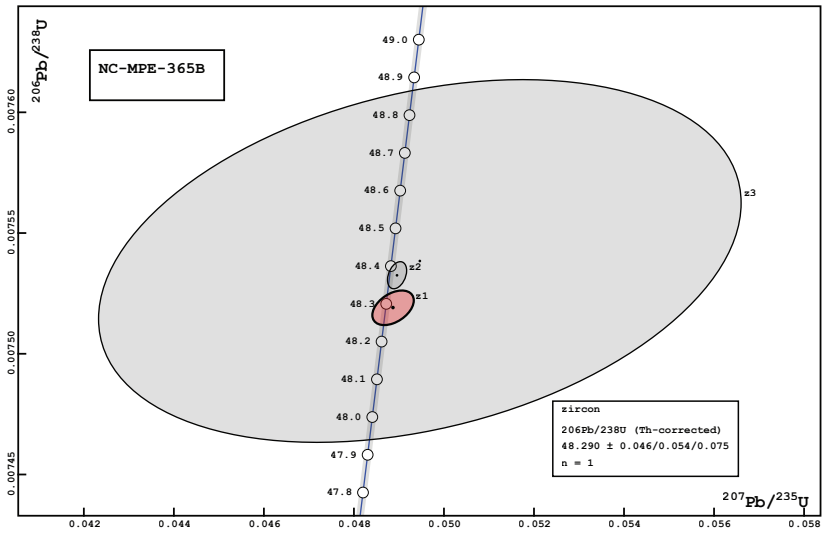
NC-MPE-365B
zircon
206Pb/238U (Th-corrected)
48.290 ± 0.046/0.054/0.075
n = 1
206Pb/238U
207Pb/235U

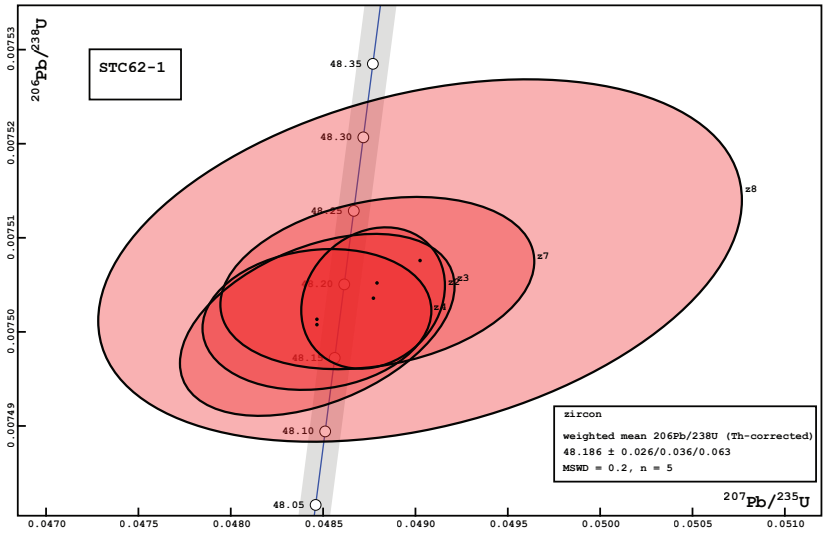
STC62-1
zircon
weighted mean 206Pb/238U (Th-corrected)
48.186 ± 0.026/0.036/0.063
MSWD = 0.2, n = 5
206Pb/238U
207Pb/235U

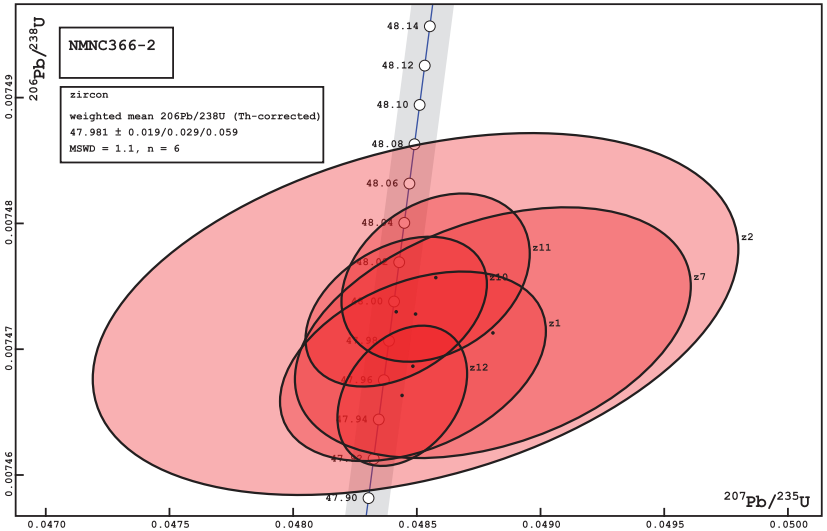
NMNC366-2
zircon
weighted mean 206Pb/238U (Th-corrected)
47.981 ± 0.019/0.029/0.059
MSWD = 1.1, n = 6
206Pb/238U
207Pb/235U

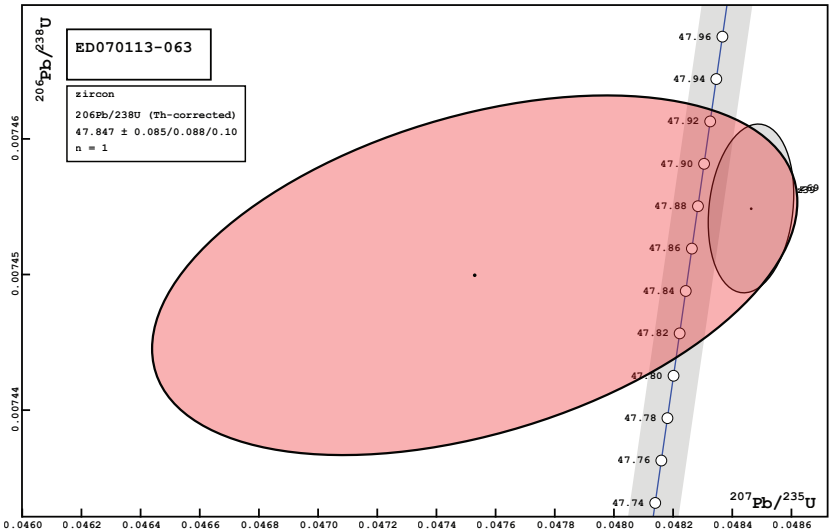
ED070113-063
zircon
206Pb/238U (Th-corrected)
47.847 ± 0.085/0.088/0.10
n = 1
206Pb/238U
207Pb/235U

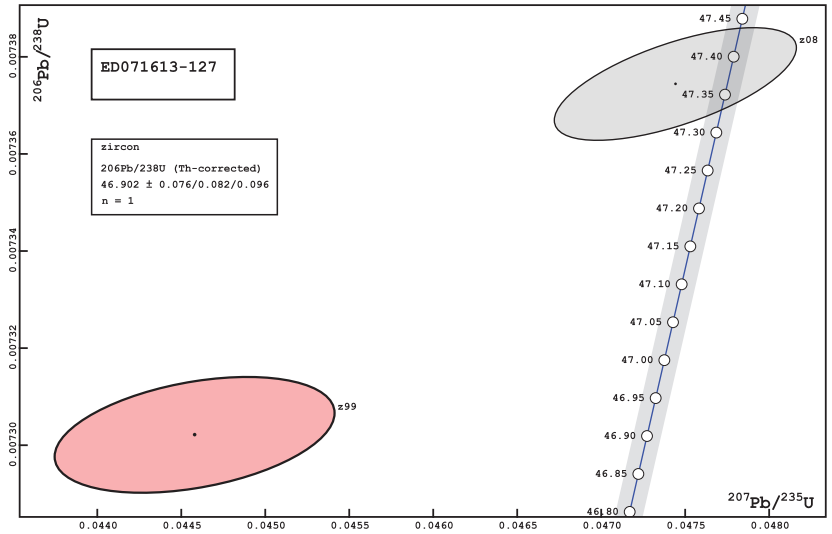
ED071613-127
zircon
206Pb/238U (Th-corrected)
46.902 ± 0.076/0.082/0.096
n = 1
z08
z99
47.45
47.40
47.35
47.30
47.25
47.20
47.15
47.10
47.05
47.00
46.95
46.90
46.85
46.80
206Pb/238U
207Pb/235U
0.00738
0.00736
0.00734
0.00732
0.00730
0.0440
0.0445
0.0450
0.0455
0.0460
0.0465
0.0470
0.0475
0.0480

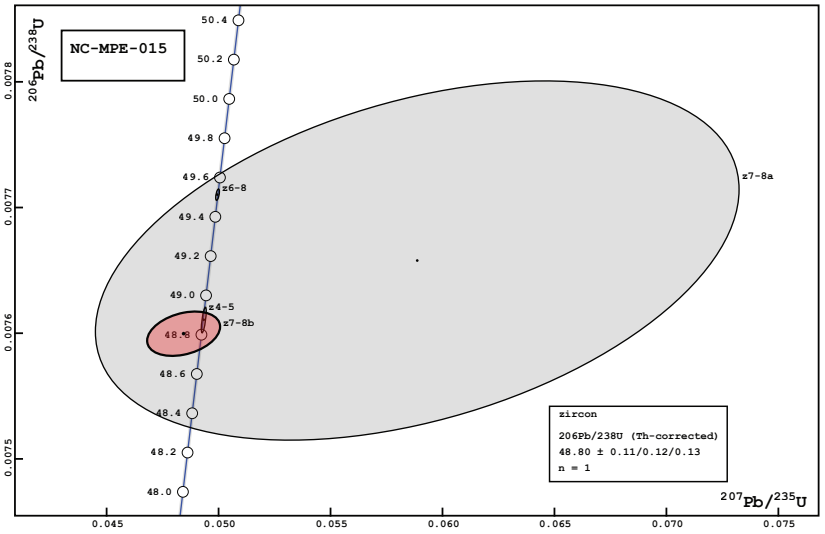
NC-MPE-015
zircon
206Pb/238U (Th-corrected)
48.80 ± 0.11/0.12/0.13
n = 1
z7-8a
z6-8
z4-5
z7-8b
50.4
50.2
50.0
49.8
49.6
49.4
49.2
49.0
48.8
48.6
48.4
48.2
48.0
206Pb/238U
207Pb/235U
0.0078
0.0077
0.0076
0.0075
0.045
0.050
0.055
0.060
0.065
0.070
0.075

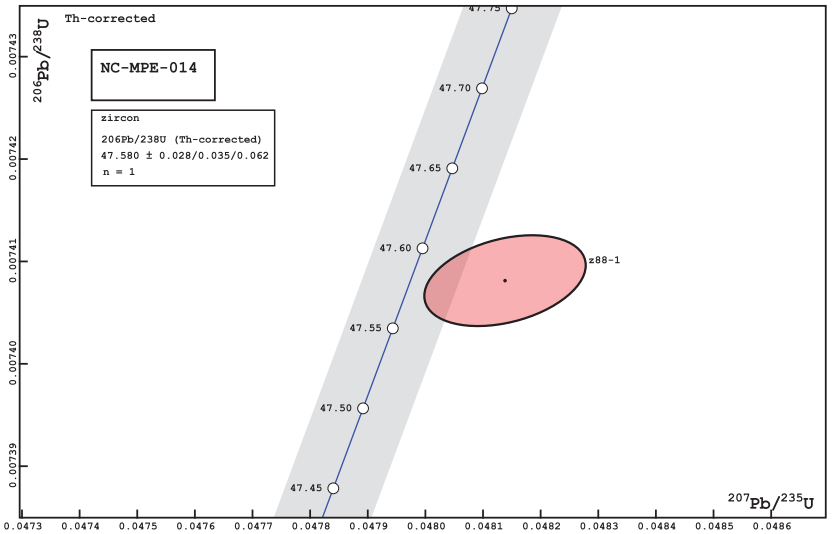
Th-corrected
NC-MPE-014
zircon
206Pb/238U (Th-corrected)
47.580 ± 0.028/0.035/0.062
n = 1
z88-1
47.70
47.65
47.60
47.55
47.50
47.45
206Pb/238U
207Pb/235U
0.00743
0.00742
0.00741
0.00740
0.00739
0.0473
0.0474
0.0475
0.0476
0.0477
0.0478
0.0479
0.0480
0.0481
0.0482
0.0483
0.0484
0.0485
0.0486

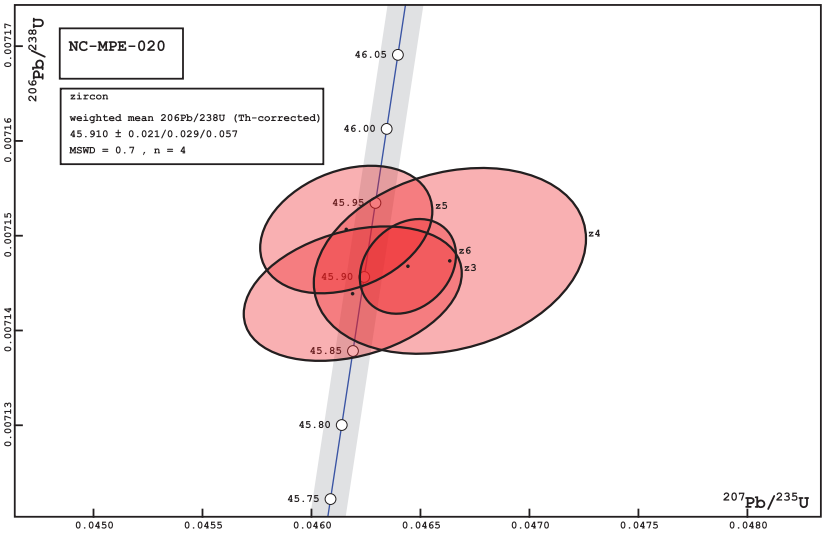
NC-MPE-020
zircon
weighted mean 206Pb/238U (Th-corrected)
45.910 ± 0.021/0.029/0.057
MSWD = 0.7 , n = 4
z5
z4
z6
z3
46.05
46.00
45.95
45.90
45.85
45.80
45.75
206Pb/238U
207Pb/235U
0.00717
0.00716
0.00715
0.00714
0.00713
0.0450
0.0455
0.0460
0.0465
0.0470
0.0475
0.0480

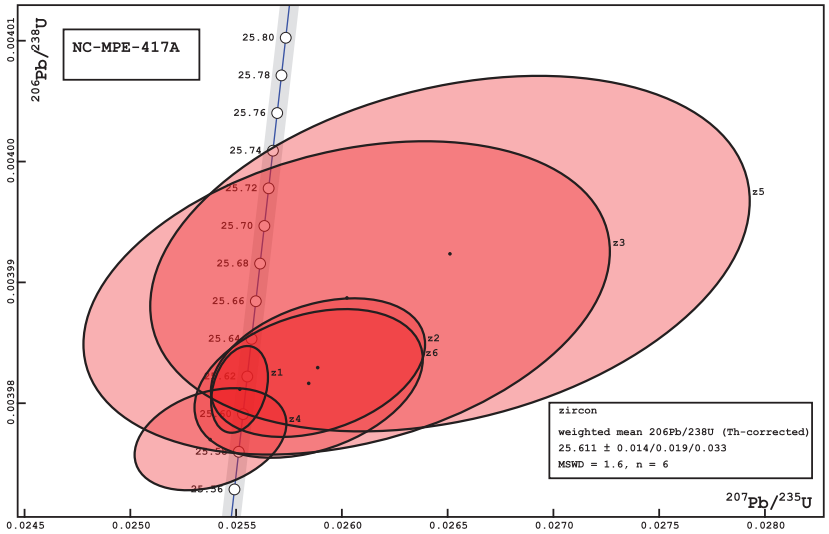
NC-MPE-417A
zircon
weighted mean 206Pb/238U (Th-corrected)
25.611 ± 0.014/0.019/0.033
MSWD = 1.6, n = 6
z1
z2
z3
z4
z5
z6
25.80
25.78
25.76
25.74
25.72
25.70
25.68
25.66
25.64
25.62
25.60
25.58
25.56
0.00401
0.00400
0.00399
0.00398
0.0245
0.0250
0.0255
0.0260
0.0265
0.0270
0.0275
0.0280
206Pb/238U
207Pb/235U

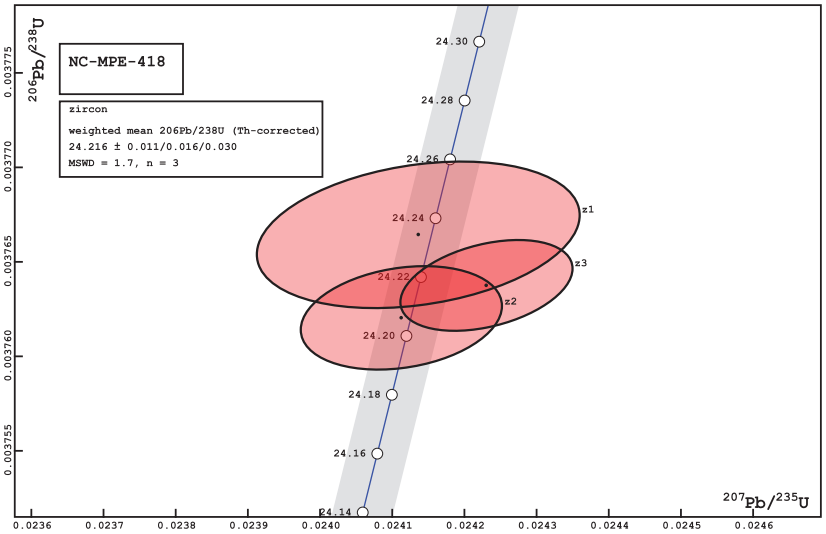
NC-MPE-418
zircon
weighted mean 206Pb/238U (Th-corrected)
24.216 ± 0.011/0.016/0.030
MSWD = 1.7, n = 3
z1
z2
z3
24.30
24.28
24.26
24.24
24.22
24.20
24.18
24.16
24.14
0.003775
0.003770
0.003765
0.003760
0.003755
0.0236
0.0237
0.0238
0.0239
0.0240
0.0241
0.0242
0.0243
0.0244
0.0245
0.0246
206Pb/238U
207Pb/235U